Lanthanide Helicates Self-Assembled in Water: A New Class of Highly Stable and Luminescent Dimetallic Carboxylates

Mourad Elhabiri,[†] Rosario Scopelliti,[†] Jean-Claude G. Bünzli,*[,†] and Claude Piguet[‡]

Contribution from the Institute of Analytical and Inorganic Chemistry, University of Lausanne, CH-1015 Lausanne, Switzerland, and Department of Inorganic, Analytical and Applied Chemistry, University of Geneva, CH-1211 Geneva 4, Switzerland

Received June 3, 1999

Abstract: The segmental ligand bis{1-ethyl-2-[6′-carboxy)pyridin-2′-yl]benzimidazol-5-yl}methane (L^C) reacts with the entire series of Ln^{III} ions to yield a new class of neutral lanthanide carboxylates, the triple-stranded dimetallic helicates $[Ln_2(L^C\text{-}2H)_3]$, which are stable in water in the pH range 4−13. A competitive titration with 1,4,7,10-tetraazacyclododecane-*N*,*N*′,*N*″,*N*‴-tetraacetic acid (dota) shows the Eu^{III} helicate to have a stability comparable to that of $[Eu(dota)]^-$. According to the X-ray structures of isotypical $[Ln_2(L^C\text{-}2H)_3]\cdot 20.5H_2O$ (Ln = Eu, Tb) ($C_{93}H_{72}Ln_2N_{18}O_{12}\cdot 20.5H_2O$, monoclinic, $P2_1/c$, $Z = 8$), the helicates are comprised of two types of slightly different molecules (A, B) within the asymmetric unit. The three ligand strands are helically wrapped around the two nine-coordinate Ln^{III} ions, leading to pseudo-D_3 symmetries around the metals. The Ln^{III}−Ln^{III} distances lie in the ranges 8.81−8.83 Å for molecules A and 9.04−9.07 Å for molecules B, while the helical pitch amounts to 23.7−23.8 Å (A) and 24.5−24.7 Å (B). In solution, the helicates retain time-averaged D_3 symmetries along the entire Ln^{III} series, as shown by ^1H and ^{13}C NMR. The derivation of equations adapted to heterodimetallic complexes allows the separation of contact and dipolar contributions to the isotropic paramagnetic shift. Somewhat different structures are evidenced between larger (Ln = Ce−Tb) and smaller (Ln = Er−Yb) Ln^{III} ions, attributed to a lengthening of the helix on going toward heavier lanthanides. The photophysical properties of the helicates depend on the nature of the Ln^{III} ion, and L^C is revealed to be a good sensitizer of Eu^{III}. The flexible route used to synthesize L^C opens interesting perspectives for the fine-tuning of the chemical and photophysical properties of lanthanide-containing homodimetallic helicates with potential applications in labeling and sensing technologies.

Introduction

Several biomedical applications of trivalent lanthanide ions, Ln^{III}, have emerged during the past two decades and pertain to three main fields:[1] (i) Gd-containing contrast agents for magnetic resonance imaging,[2] (ii) catalysts for the cleavage of phosphate diester bridges in DNA and RNA,[3] and (iii) luminescent stains for protein labeling and sensitive homogeneous immunoassays.[4,5] Luminescent signals being among the most sensitive to detect, the selection of luminescent labels for immunoassays was straightforward, despite intrinsic limitations due to the assay medium, namely nonspecific short-lived luminescence, and to the modulation of the label's signal, which should be independent of the substrate. The former drawback can be mastered by the use of lanthanide chelates displaying long-lived luminescence (0.01−1 ms) and allowing time-resolved measurements with concomitant elimination of the background noise.[4,5]

Lanthanide luminescent labels must fulfill several restrictive requirements: (i) good thermodynamic and kinetic stabilities under physiological conditions, (ii) the ability to easily couple with biological materials, and (iii) specific photophysical properties. Since f−f transitions are very weak, excitation usually relies on energy transfer from the ligands surrounding the lanthanide ion (antenna effect[6]). In addition to efficient sensitization, the design of lanthanide-containing luminescent stains has to overcome another difficulty, arising from the easy de-excitation of the Ln^{III} excited states through high-energy vibrations[7] or low-lying ligand-to-metal charge-transfer (LMCT) states.[8−10] One tactics to solve these problems relies on the encapsulation of the Ln^{III} ions in supramolecular edifices, providing a rigid and protective environment for the metal ion. This is achieved by using preorganized macrocyclic ligands,[11] multidentate podands,[12] or self-assembly processes[13] which

[†] University of Lausanne.
[‡] University of Geneva.

(1) *Lanthanide Probes in Life, Chemical and Earth Sciences: Theory and Practice*; Bünzli, J.-C. G., Choppin, G. R., Eds; Elsevier Science Publ. B.V.: Amsterdam, 1989.
(2) Lauffer, R. B. In *MRI Clinical Magnetic Resonance Imaging*; Edelman, R. E., Zlatkin, M. B., Hesselink, J. R., Eds.; W. B. Saunders Co.: Philadelphia, 1996.
(3) Roigk, A.; Hettich, R.; Schneider, H.-J. *Inorg. Chem.* **1998**, *37*, 751.
(4) Hemmilä, I.; Ståhlberg, T.; Mottram, P. *Bioanalytical Applications of Labelling Technologies*; Wallac Oy: Turku, 1995.
(5) Mathis, G. In *Rare Earths*; Saez Puche, R., Caro, P., Eds; Editorial Complutense: Madrid, 1998.
(6) Sabbatini, N.; Perathoner, S.; Balzani, V.; Alpha, B.; Lehn, J.-M. In *Supramolecular Chemistry*; Balzani, V., Ed.; D. Reidel Publishing Co.: Dordrecht, 1987.
(7) Haas, Y.; Stein, G. *J. Phys. Chem.* **1971**, *75*, 3668.
(8) Blasse, G. *Phys. Status Solidi A* **1992**, *130*, K85.
(9) Bünzli, J.-C. G.; Froidevaux, P.; Harrowfield, J. M. *Inorg. Chem.* **1993**, *32*, 3306.
(10) Petoud, S.; Glanzmann, T.; Bünzli, J.-C. G.; Piguet, C.; Qin, X.; Thummel, R. P. *J. Luminesc.* **1999**, *82*, 69.
(11) Alexander, V. *Chem. Rev.* **1995**, *95*, 273.
(12) Jones, P. L.; Amoroso, A. J.; Jeffery, J. C.; McCleverty, J. A.; Psillakis, E.; Rees; L. H.; Ward, M. D. *Inorg. Chem.* **1997**, *36*, 10.
(13) Lehn, J.-M. *Supramolecular Chemistry. Concepts and Perspectives*; VCH: Weinheim, 1995.

10.1021/ja991854q CCC: $18.00
Published on Web 11/04/1999

Chart 1

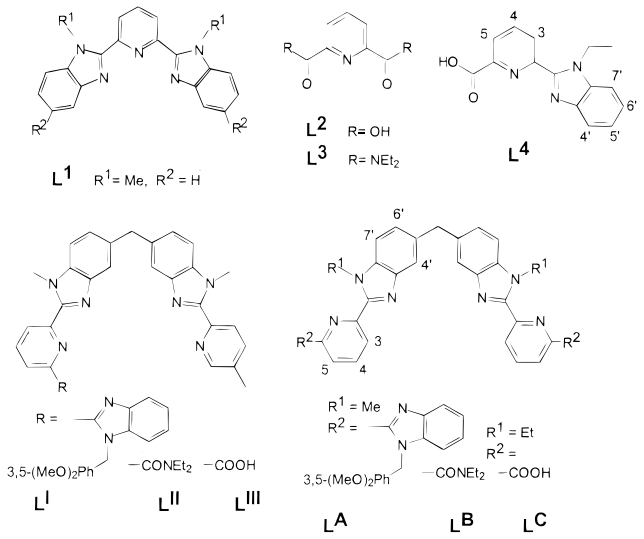

allow the fine-tuning of the Ln^{III} coordination sphere. In recent years, we have pursued a research program based on the induced-fit concept[14] and using ligands derived from bis(benzimidazole)pyridine in order to prepare lanthanide-containing supramolecular precursors for functional devices.[15] Simple symmetric tridentate receptors L^1 (Chart 1) give stable and inert triple-helical complexes $[Ln(L^1)_3]^{3+}$ in acetonitrile,[16,17] displaying a substantial ion-size discriminating effect,[18] while the addition of semirigid lipophilic substituents in position R^2 leads to mesogenic ligands and U-shaped 1:1 nitrato complexes.[19] Unsymmetrical ditopic ligands L^I-L^{III} provide heterodimetallic noncovalent Ln^{III} podates $[LnM(L)_3]^{5+}$ (M = Zn,[20−22] Fe,[23,24] Co[25]) which are building blocks for luminescent (Zn) and magnetic (Fe, Co) materials.[15] Recently, it has been realized that dimetallic lanthanide edifices offer improved possibilities for the catalytic cleavage of RNA[26,27] and for the design of calcium-triggered Gd^{III} MRI contrast agents.[28] Moreover, dimetallic complexes with luminescent Ln^{III} ions have the potential advantage of combining two stains in a small volume, and the symmetrical ditopic ligands L^A [29] and L^B [30] have been designed for the self-assembly of the cationic triple-stranded helicates[31] $[Ln_2(L^{A,B})_3]^{6+}$ in acetonitrile. Yet, bioanalytical applications require water-soluble probes, and in order to test whether the energetic drive leading to the formation of dimetallic helicates in water is able to compensate the large dehydration enthalpy of the lanthanide aquo ions (3640−3760 kJ·mol^{-1} for 4f ions[32] vs 1850−2105 kJ·mol^{-1} for divalent 3d transition metal ions), we have introduced two carboxylic acid functions in L^C,[33] leading to stable, water-soluble and neutral triple-stranded helicates $[Ln_2(L^C\text{-}2H)_3]$. In this paper, we present a structural, thermodynamic, and photophysical study of the neutral $[Ln_2(L^C\text{-}2H)_3]$ helicates both in the solid state and in water (Ln = Y, La−Nd, Sm−Tb, Er−Lu). These assemblies represent a new class of versatile water-soluble lanthanide carboxylates whose electronic and luminescent properties can be easily tuned by modifying the attached substituents. A preliminary account of this work has been reported elsewhere.[33]

Experimental Section

Solvents and starting materials were purchased from Fluka AG (Buchs, Switzerland) and used without further purification, unless otherwise stated. Acetonitrile, dichloromethane, *N*,*N*-dimethylformamide (DMF), and triethylamine were distilled from CaH_2; thionyl chloride was distilled from elemental sulfur. Silicagel (Merck 60, 0.04−0.06 mm) was used for preparative column chromatography. The perchlorate salts $Ln(ClO_4)_3 \cdot nH_2O$ (Ln = La to Lu) were prepared from corresponding oxides (Rhône-Poulenc, 99.99%) in the usual way.[34] ***Caution!*** *Perchlorate salts combined with organic ligands are potentially explosive and should be handled in small quantities and with adequate precautions.*[35]

Preparation of the Ligands. 2,6-Pyridinedicarboxylic acid monomethyl ester (**1**),[36] 3,3′-dinitro-4,4′-bis(*N*-ethylamino)diphenylmethane (**3**),[37] diethyl-*N*,*N*′-[methylenebis(2-nitrophen-4,1-ylene)]bis[6-(*N*,*N*-diethylcarbamoyl)pyridine-2-carboxamide] (**4**),[30] bis{1-alkyl-2-[6′-(*N*,*N*-diethylcarbamoyl)pyridin-2′-yl]benzimidazol-5-yl}methane (L^B),[30] and *N*-ethyl-2-nitroaniline (**5**)[38] were prepared according to literature procedures.

Preparation of 6-(*N*,*N*-Diethylcarbamoyl)pyridine-2-carboxylic Acid (2). A mixture of 2,6-pyridinedicarboxylic acid monomethyl ester (**1**, 1.3 g, 7.18 mmol), freshly distilled thionyl chloride (34.16 g, 0.287 mmol), and DMF (100 μL) was refluxed for 60 min in dry dichloromethane (50 mL). The mixture was evaporated and dried under vacuum for 30 min, and the resulting solid was dissolved in dry dichloromethane (50 mL). Dry *N*,*N*-diethylamine (5.25 g, 71.8 mmol) was added dropwise under an inert atmosphere. The resulting solution was refluxed for 90 min and evaporated. The brown crude residue was partitioned between dichloromethane (100 mL) and half-saturated aqueous NH_4Cl solution (100 mL). The aqueous phase was extracted with dichloromethane (2 × 100 mL), and the combined organic phases were washed with a saturated $KHCO_3$ solution (2 × 100 mL), dried (Na_2SO_4), and evaporated to dryness. The resulting brown solid was dissolved in 1 M KOH solution (50 mL) and stirred at room temperature for 10 min. The aqueous phase was extracted with chloroform (2 × 50

(14) Koshland, D. E., Jr. *Angew. Chem., Int. Ed. Engl.* **1994**, *33*, 2375.
(15) Piguet, C.; Bünzli, J.-C. G. *Chimia* **1998**, *52*, 579.
(16) Piguet, C.; Williams, A. F.; Bernardinelli, G.; Bünzli, J.-C. G. *Inorg. Chem.* **1993**, *32*, 4139.
(17) Piguet, C.; Bünzli, J.-C. G.; Bernardinelli, G.; Bochet, C. G.; Froidevaux, P. *J. Chem. Soc., Dalton Trans.* **1995**, 83.
(18) Petoud, S.; Bünzli, J.-C. G.; Renaud, F.; Piguet, C.; Schenk, K. J.; Hopfgartner, G. *Inorg. Chem.* **1997**, *36*, 5750.
(19) Nozary, H.; Piguet, C.; Tissot, P.; Bernardinelli, G.; Bünzli, J.-C. G.; Deschenaux, R.; Guillon, D. *J. Am. Chem. Soc.* **1998**, *120*, 12274.
(20) Piguet, C.; Rivara-Minten, E.; Hopfgartner, G.; Bünzli, J.-C. G. *Helv. Chim. Acta* **1995**, *78*, 1541.
(21) Piguet, C.; Bünzli, J.-C. G.; Bernardinelli, G.; Hopfgartner, G.; Petoud, S.; Schaad, O. *J. Am. Chem. Soc.* **1996**, *118*, 6681.
(22) Edder, C.; Piguet, C.; Bünzli, J.-C. G.; Hopfgartner, G. *J. Chem. Soc., Dalton Trans.* **1997**, 4657.
(23) Piguet, C.; Rivara-Minten, E.; Hopfgartner, G.; Bünzli, J.-C. G. *Helv. Chim. Acta* **1995**, *78*, 1651.
(24) Piguet, C.; Rivara-Minten, E.; Bernardinelli, G.; Bünzli, J.-C. G.; Hopfgartner, G. *J. Chem. Soc., Dalton Trans.* **1997**, 421.
(25) Rigault, S.; Piguet, C.; Bernardinelli, G.; Hopfgartner, G. *Angew. Chem., Int. Ed. Engl.* **1988**, *27*, 169.
(26) Hurst, P.; Takasaki, B. K.; Chin, J. *J. Am. Chem. Soc.* **1996**, *118*, 9982.
(27) Bruice, T. C.; Tsubouchi, A.; Dempey, R. O.; Olson, L. P. *J. Am. Chem. Soc.* **1996**, *118*, 9867.
(28) Li, W. H.; Fraser, S. E.; Meade, T. J. *J. Am. Chem. Soc.* **1999**, *121*, 1413.
(29) Piguet, C.; Bünzli, J.-C. G.; Bernardinelli, G.; Hopfgartner, G.; Williams, A. F. *J. Am. Chem. Soc.* **1993**, *115*, 8197.
(30) Martin, N.; Bünzli, J.-C. G.; McKee, V.; Piguet, C.; Hopfgartner, G. *Inorg. Chem.* **1998**, *37*, 577.
(31) Piguet, C.; Bernardinelli, G.; Hopfgartner, G. *Chem. Rev.* **1997**, *97*, 2005.
(32) Bünzli, J.-C. G. In *Rare Earths*; Saez Puche, R., Caro, P., Eds.; Editorial Complutense: Madrid, 1998.
(33) Elhabiri, M.; Scopelliti, R.; Bünzli, J.-C. G.; Piguet, C. *Chem. Commun.* **1998**, 2347.
(34) Desreux, J. F. In *Lanthanide Probes in Life, Chemical and Earth Sciences. Theory and Practice*; Bünzli, J.-C. G., Choppin, G. R., Eds.; Elsevier Science Publ. B.V.: Amsterdam, 1989.
(35) Raymond, K. N. *Chem. Eng. News* **1983**, *61* (49), 4.
(36) Johansen, J. E.; Christie, B. D.; Rapoport, H. *J. Org. Chem.* **1981**, *46*, 4914.
(37) Piguet, C.; Bernardinelli, G.; Bocquet, B.; Quattropani, A.; Williams, A. F. *J. Am. Chem. Soc.* **1992**, *114*, 7440.
(38) Lamm, B. *Acta Chem. Scand.* **1965**, *19*, 2316.

mL), acidified to pH = 2 with hydrochloric acid (25%), concentrated, and cooled at 0 °C for 12 h. White crystals were collected by filtration and recrystallized from hot acetonitrile to give 1.3 g (5.85 mmol, yield 81.5%) of **2**. ^{1}H NMR in CD_3OD: δ 1.23 (3H, t, J^3 = 7 Hz), 1.32 (3H, t, J^3 = 7 Hz), 3.37 (2H, q, J^3 = 7 Hz), 3.62 (2H, q, J^3 = 7 Hz), 7.80 (1H, dd, J^3 = 8 Hz, J^4 = 1.3 Hz), 8.15 (1H, t, J^3 = 8 Hz), 8.26 (1H, dd, J^3 = 8 Hz, J^4 = 1.3 Hz). ^{13}C NMR in CD_3OD: δ 13.21, 14.62 (primary C); 41.82, 45.07 (secondary C); 126.99, 127.30, 140.35 (tertiary C); 148.81, 156.16, 167.62 (quaternary C). ESI-MS (CH_3CN): *m*/*z* 220.7 $[M + H]^+$, 281.0 $([M + H + CH_3CN + H_2O]^+$.

Preparation of *Bis*{1-ethyl-2-[(6′-carboxy)pyridin-2′-yl]benzimidazol-5-yl}methane (L^C). A solution of L^B (300 mg, 0.46 mmol) in 250 mL of ethanol/water 1:4 containing potassium hydroxide (86%, 15.13 g, 230 mmol) was refluxed for 12 h. Ethanol was distilled off, and the aqueous phase was acidified to pH = 3 with concentrated hydrochloric acid (25%). The resulting precipitate was filtered off and washed with water to give 235 mg (0.43 mmol, yield 93.5%) of L^C as a white powder. ESI-MS (CH_3CN): *m*/*z* 547.5 $([M + H]^+)$, 588.8 $([M + H + CH_3CN]^+)$, 607.4 $([M + H + CH_3CN + H_2O]^+)$. Elemental analysis: see Table S1, Supporting Information.

Preparation of 2-(*N*,*N*-Diethylcarbamoyl)-6-(1′-ethyl-1*H*-benzimidazol-2′-yl)pyridine (6). 6-(*N*,*N*-Diethylcarbamoyl)pyridine-2-carboxylic acid (**2**, 1 g, 4.5 mmol), freshly distilled thionyl chloride (21.4 g, 180 mmol), and DMF (100 μL) in dry dichloromethane (35 mL) were refluxed for 90 min. The mixture was evaporated to dryness and dried under vacuum for 1 h. The resulting pale yellow solid was dissolved in dry dichloromethane (40 mL), and a mixture of 2-nitro-*N*-ethylaniline (**5**, 748 mg, 4.50 mmol) and triethylamine (4.55 g, 45 mmol) in dry dichloromethane (30 mL) was added dropwise under an inert atmosphere. The solution was refluxed for 90 min and evaporated. The brown residue was partitioned between dichloromethane (100 mL) and half-saturated aqueous NH_4Cl solution (100 mL). The aqueous phase was extracted with dichloromethane (2 × 100 mL), and the combined organic phases were washed with a saturated $KHCO_3$ solution (2 × 100 mL), dried over Na_2SO_4, and evaporated. The crude product was dissolved in a mixture of 220 mL of EtOH and 55 mL of H_2O, and freshly activated iron powder (5.28 g, 94.5 mmol) and concentrated HCl (25%, 30.6 mL, 236 mmol) were added. The mixture was refluxed for 8 h under an inert atmosphere. The excess of iron was filtered off, and ethanol was distilled off under vacuum. Water was added to bring the total volume to 100 mL. The resulting mixture was poured into dichloromethane (150 mL), $Na_2H_2EDTA{\cdot}2H_2O$ (40 g in 250 mL of H_2O) was added, and the resulting stirred mixture was neutralized to pH = 7 with 5 M aqueous KOH. Concentrated H_2O_2 (30%, 2 mL) was then added under vigorous stirring, and the pH was adjusted to 8.5. After 30 min, the organic layer was separated and the aqueous phase extracted with dichloromethane (3 × 150 mL). The combined organic phases were dried over Na_2SO_4 and evaporated. The resulting brown crude solid was purified by column chromatography (silica gel, CH_2Cl_2/MeOH 100:0 → 98:2) to give 818 mg (2.54 mmol, 56.4%) of **6**. ^{1}H NMR in $CDCl_3$: δ 1.05 (3H, t, J^3 = 7 Hz), 1.27 (3H, t, J^3 = 7 Hz), 1.46 (3H, t, J^3 = 7.9 Hz), 3.34 (2H, q, J^3 = 7.1 Hz), 3.60 (2H, q, J^3 = 7.1 Hz), 4.75 (2H, q, J^3 = 8 Hz), 7.31 (2H, m), 7.44 (1H, d, J^3 = 7 Hz), 7.54 (1H, d, J^3 = 8 Hz), 7.83 (1H, d, J^3 = 7 Hz), 7.92 (1H, t, J^3 = 8 Hz), 8.38 (1H, d, J^3 = 8 Hz). ^{13}C NMR in $CDCl_3$: δ 13.43, 14.91, 15.96 (primary C); 40.16, 41.13, 43.42 (secondary C); 110.72, 120.81, 123.11, 123.32, 124.13, 125.60, 138.58 (tertiary C); 136.86, 143.35, 149.92, 150.03, 155.09, 169.07 (quaternary C). ESI-MS (CH_3CN): *m*/*z* 322.8 $([M + H]^+)$, 364.0 $([M + H + CH_3CN]^+)$, 383.3 $([M + H + CH_3CN + H_2O]^+)$.

Preparation of 6-(1′-Ethylbenzimidazol-2′-yl)pyridine-2-carboxylic Acid (L^4). A solution of **6** (600 mg, 1.86 mmol) in 250 mL of ethanol/water 1:4 containing potassium hydroxide (86%, 60.7 g, 930 mmol) was refluxed for 12 h. Ethanol was distilled off, and the aqueous phase was acidified to pH = 3 with concentrated HCl (25%). The resulting precipitate was filtered off and washed with H_2O to give 456 mg (1.70 mmol, yield 92%) of L^4 as a white powder. ^{1}H NMR in DMSO-d_6: δ 1.43 (3H, t, J^3 = 7 Hz), 4.91 (2H, q, J^3 = 7.1 Hz), 7.29 (1H, td, J^3 = 7.1 Hz, J^4 = 1.3 Hz), 7.35 (1H, td, J^3 = 7.1 Hz, J^4 = 1 Hz), 7.69 (1H, d, J^3 = 7.9 Hz), 7.75 (1H, d, J^3 = 7.9 Hz), 8.14 (1H, dd, J^3 = 7.9 Hz, J^4 = 1.6 Hz), 8.17 (1H, t, J^3 = 7.7 Hz), 8.52 (1H, dd, J^3 = 7.4 Hz, J^4 = 1.7 Hz). ^{13}C NMR in DMSO-d_6: δ 19.33 (primary C); 44.08 (secondary C); 114.76, 123.67, 126.50, 127.47, 128.85, 130.83, 142.71 (tertiary C); 140.14, 146.15, 151.82, 152.33, 153.79, 169.94 (quaternary C). ESI-MS (CH_3OH): *m*/*z* 267.7 $([M + H]^+)$, 299.8 $([M + H + CH_3OH]^+)$, 308.9 $([M + H + CH_3CN]^+)$. Elemental analysis: see Table S1, Supporting Information.

Preparation of the Complexes $[Ln_2(L^C\text{-}2H)_3]{\cdot}nH_2O$ (Ln = La, 7; Ce, 8; Pr, 9; Nd, 10; Sm, 11; Y, 12; Eu, 13; Gd, 14; Tb, 15; Er, 16; Tm, 17; Yb, 18; Lu, 19). A solution of L^C (30 mg, 0.052 mmol) in freshly distilled DMF (4 mL) was stirred at 50 °C for 1 h. Triethylamine was added dropwise, and the mixture was stirred at 50 °C for 20 min. A solution of $Ln(ClO_4){\cdot}nH_2O$ (Ln = La, Pr, Nd, Sm, Y, Eu, Gd, Tb, Er, Tm, Yb, Lu; n = 2−9, 0.035 mmol) or $Ce(CF_3SO_3)_3{\cdot}8.5H_2O$ (0.035 mmol) in 120 μL of distilled DMF was added dropwise, and the mixture was stirred for 1 h at 50 °C. The resulting white precipitate was filtered off, washed successively with DMF and CH_3CN, and recrystallized from hot water. Colorless crystalline solids were isolated by filtration and dried under vacuum (10^{-2} mmHg) at 60 °C for 24 h to give complexes $[Ln_2(L^C\text{-}2H)_3]{\cdot}nH_2O$ (Ln = La (n = 8), Ce, (n = 8), Pr (n = 6), Nd (n = 14), Sm (n = 16), Y (n = 16), Eu (n = 9), Gd (n = 19), Tb (n = 15), Er (n = 8), Tm (n = 11), Yb (n = 13), and Lu (n = 14)). X-ray-quality crystals of $[Eu_2(L^C\text{-}2H)_3]{\cdot}20.5H_2O$ (**13a**) were obtained by slow evaporation of a concentrated aqueous solution. X-ray-quality crystals of $[Tb_2(L^C\text{-}2H)_3]{\cdot}20.5H_2O$ (**15a**) were grown by slow diffusion of acetone into a concentrated aqueous solution. Complexes **7**−**19** gave satisfactory elemental analyses and were further characterized by their IR spectra (see Tables S1 and S2, Supporting Information).

Preparation of Eu-Doped $[Ln_2(L^C\text{-}2H)_3]{\cdot}nH_2O$ (Ln = La, 20 (n = 12); Lu, 21 (n = 20)); Tb, 22 (n = 14)). For the photophysical study, Eu-doped (2%) complexes were prepared by replacing the lanthanide solution by a Ln (98%)/Eu (2%) mixed solution for **20** and **21** and by a Tb (50%)/Eu (50%) mixed solution for **22**.

Spectroscopic and Analytical Measurements. IR and UV−vis measurements were performed as described earlier.[30] In a typical spectrophotometric titration, 25 samples were prepared 24 h in advance to ensure that equilibrium had been reached, with $[L^C]_{tot}$ between 1.6×10^{-5} and 1.5×10^{-5} M and $[Ln^{III}]_{tot}$ between 4.3×10^{-7} and 1.6×10^{-5} M. Plots of molar absorption coefficient as a function of the metal/ligand ratio and factor analysis[39] were used to determine a suitable model, and the data were fitted with the SPECFIT program.[40] Potentiometric measurements were carried out with an automated Metrohm Titrino 736 GP potentiometer (resolution 0.1 mV, accuracy 0.2 mV) using a volume addition program. An automated buret (Metrohm 6.3013.210, 10 mL, accuracy 0.03 mL), was used, along with a Metrohm 6.0204.100 glass electrode. ^{1}H NMR spectra were recorded at 25 °C on a Bruker AM360 or a Bruker AVANCE DRX400 spectrometer. Chemical shifts are reported in parts per million with respect to TMS. Mass spectra were obtained by electron spray ionization (ESI-MS) on a Finnigan LC 710 spectrometer. The experimental procedures for high-resolution, laser-excited luminescence studies have been published previously.[41] Quantum yields have been determined according to the procedure described in ref 10 (refractive indices used: 1.333 and 1.329 for solutions in H_2O and MeOH, respectively). Ligand-centered luminescence was measured relative to quinine sulfate in 0.05 M H_2SO_4 (n = 1.338, absolute yield 0.546, ref 42). Metal-centered luminescence was determined with respect to solutions of $[Ln(tpy)_3](ClO_4)_3$ 10^{-3} M in MeCN (n = 1.343, absolute quantum yield 0.013 for Eu[43] and 0.047 for Tb[44]); tpy stands for 2,2′:6′,2″-terpyridine. Degassed solvents for spectroscopy were used, and experimental conditions were set to minimize self-absorption and guarantee a linear

(39) Malinowski, E. R.; Howery, D. G. *Factor Analysis in Chemistry*; John Wiley: New York, 1980.
(40) Gampp, H.; Maeder, M.; Meyer, C. J.; Zuberbühler, A. D. *Talanta* **1985**, *32*, 257.
(41) Piguet, C.; Williams, A. F.; Bernardinelli, G.; Moret, E.; Bünzli, J.-C. G. *Helv. Chim. Acta* **1992**, *75*, 1697.
(42) Meech, S. R.; Phillips, D. C. *J. Photochem.* **1983**, *23*, 193.
(43) Petoud, S.; Bünzli, J.-C. G.; Schenk, K. J.; Piguet, C. *Inorg. Chem.* **1997**, *36*, 1345.
(44) Charbonnière, L. J.; Balsiger, C.; Schenk, K. J.; Bünzli, J.-C. G. *J. Chem. Soc., Dalton Trans.* **1998**, 505.

Table 1. Summary of Crystal Data, Intensity Measurements, and Structure Refinements for $[Eu_2(L^C\text{-}2H)_3]\cdot 20.5H_2O$ (**13a**) and $[Tb_2(L^C\text{-}2H)_3]\cdot 20.5H_2O$ (**15a**)

	$[Eu_2(L^C\text{-}2H)_3]\cdot 20.5H_2O$	$[Tb_2(L^C\text{-}2H)_3]\cdot 20.5H_2O$
formula	$C_{93}H_{72}Eu_2N_{18}O_{12}\cdot 20.5H_2O$	$C_{93}H_{72}Tb_2N_{18}O_{12}\cdot 20.5H_2O$
mol wt	2306.93	2320.85
crystal syst	monoclinic	monoclinic
space group	$P2_1/c$	$P2_1/c$
a, Å	24.808(10)	24.844(3)
b, Å	36.285(10)	36.187(3)
c, Å	23.701(10)	23.741(5)
β, deg	110.30(3)	110.65(2)
V, Å^3	20009(13)	19973(5)
Z	8	8
$F(000)$	9464	9496
D_c/Mg m^{-3}	1.532	1.544
μ(Mo Kα), mm^{-1}	1.333	1.496
cryst size, mm	0.31 × 0.24 × 0.18	0.50 × 0.42 × 0.24
temp, K	185	173
no. of reflns measd	93 431	200 563
θ range	$1.04 < 2\theta < 24.40$	$0.88 < 2\theta < 27.51$
hkl ranges	$-27 < h < 27$	$-32 < h < 32$
	$-40 < k < 42$	$-46 < k < 46$
	$-27 < l < 25$	$-30 < l < 30$
no. of unique reflns	28 393	42 101
no. of reflns obsd $I > 2\sigma(I)$	15 976	26 263
no. of parameters	2630	2630
$R1$ [$I > 2\sigma(I)$][a]	0.0609	0.0549
weight	$1/(\sigma^2(F_0) + (0.0943P)^2)^b$	$1/(\sigma^2(F_0) + (0.0929P)^2)^b$
w$R2$[c]	0.1714	0.1567
max Fourier diff, e/Å^3	1.163, −1.146	1.877, −1.463

[a] $R1 = \sum||F_o| - |F_c||/\sum|F_o|$. [b] $P = (F_o^2 + 2F_c^2)/3$. [c] $wR2 = \{\sum[w(F_o^2 - F_c^2)^2]/\sum[w(F_o^2)^2]\}^{1/2}$.

relationship between the emitted light and the concentration. Elemental analyses were performed by Dr. H. Eder from the Microchemical Laboratory of the University of Geneva.

X-ray Crystal Structure Determination of $[Ln_2(L^C\text{-}2H)_3]\cdot 20.5H_2O$ (Ln = Eu, 13a; Tb, 15a). A summary of the crystal data, intensity measurements, and structure refinements is reported in Table 1. Crystals of **13a** and **15a** were mounted in glass capillaries and sealed under nitrogen. Diffraction data for both complexes have been collected on a mar345 image plate detector at 185 (**13a**) and 173 K (**15a**) and reduced with the marHKL program, release 1.9.1.[45] No absorption correction was applied. Structure solution for both compounds was performed with ab initio direct methods.[46] All structures were refined using the full-matrix block least-squares on F^2 with all non-H atoms anisotropically defined. H atoms were placed in calculated positions using the "riding model" with a common isotropic displacement parameter ($U_{iso} = 0.08$ Å^2). The only problem in both structures was a disordered water molecule (O52), for which two different (A and B) positions were refined. Structure solution, refinement, molecular graphics, and geometrical calculation have been carried out with the SHELXTL software package, release 5.1 (Bruker AXS, Inc., Madison, WI, 1997). Final atomic coordinates with equivalent isotropic displacement parameters (Table S3), anisotropic displacement parameters (Table S4), and X-ray crystallographic data (CIF) for **15a** are listed in the Supporting Information. Data for **13a** have been already deposited (CCDC 182/1036, Cambridge Crystallographic Data Center).[33]

Results

Ligand Synthesis and Properties. Bis{1-ethyl-2-[(6′-carboxy)pyridin-2′-yl]benzimidazol-5-yl}methane (L^C) was obtained in good yield by a four-step procedure involving a modified double Phillips coupling reaction to form the benzimidazole units (Scheme 1).[47] The novelty of this strategy is the synthesis of the unsymmetrical synthon 6-(*N*,*N*-diethylcarbamoyl)pyridine-2-carboxylic acid (**2**) from the monoester **1**, which is obtained via a statistical esterification of pyridine-2,6-dicarbocylic acid.[36] As the direct reaction of pyridine-2,6-dicarboxylic acid with a stoichiometric amount of trifluoroacetic anhydride followed by treatment with amines produces significant quantities of diamide and unreacted material,[48] we had first developed an approach based on the amidation of 6-methylpyridine-2-carboxylic acid, followed by the oxidation of the methyl group by anhydrous selenium dioxide in dry pyridine.[21] The new method proposed here uses less toxic reagents, produces **2** in much better yield, and can be easily extended to obtain asymmetric pyridine rings substituted in the 4-position. The tridentate monocarboxylic ligand L^4 has been synthesized for comparison purposes (Scheme 2).

Scheme 1[a]

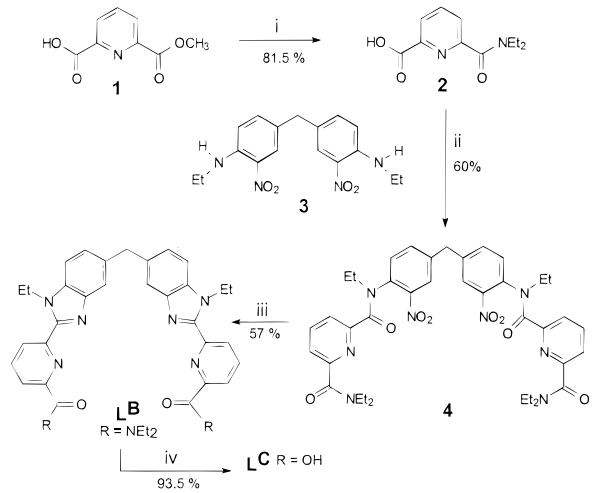

[a] Reagents: (i) $SOCl_2$, CH_2Cl_2, DMF_{cat}, $HNEt_2$, then KOH, H_2O; (ii) $SOCl_2$, CH_2Cl_2, DMF_{cat}, then **3**, NEt_3; (iii) Fe, HCl, EtOH−H_2O; (iv) KOH, EtOH−H_2O, then HCl.

Scheme 2[a]

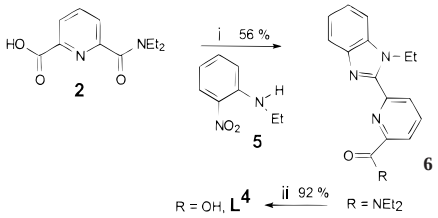

[a] Reagents: (i) (1) $SOCl_2$, CH_2Cl_2, DMF_{cat}; (2) **5**, NEt_3; (3) Fe, HCl, EtOH−H_2O; (ii) KOH, EtOH−H_2O.

The dicarboxylic ligand L^C is soluble in DMSO and DMF but is sparingly soluble in water at acidic pH's, and precipitation occurs below pH = 4. However, when the pH is increased, deprotonation occurs, and the solubility becomes quite sizable at pH > 9. Potentiometric titration of 9.4×10^{-5} M L^C (starting pH = 10.3) with perchloric acid revealed two distinct equivalent points in the region where no precipitation occurs, each one corresponding to the neutralization of 1 equiv of carboxylate and corresponding to pK_a's of 4.42 ± 0.04 and 7.7 ± 0.1 (292 K, 0.1 M Et_4NClO_4). A spectrophotometric titration conducted

(45) Otwinowski, Z.; Minor, W. In *Macromolecular Crystallography, Part A*; Carter, C. W., Jr., Sweet, R. M., Eds.; Academic Press: New York, 1997.

(46) Sheldrick, G. M. *Acta Crystallogr.* **1997**, *A46*, 467.

(47) Piguet, C.; Bocquet, B.; Hopfgartner, G. *Helv. Chim. Acta* **1994**, *77*, 931.

(48) Reddy, K. V.; Jin, S.-J.; Arora, P. K.; Sfeir, D. S.; Maloney, S. C. F.; Urbach, F. L.; Sayre, L. M. *J. Am. Chem. Soc.* **1990**, *112*, 2332.

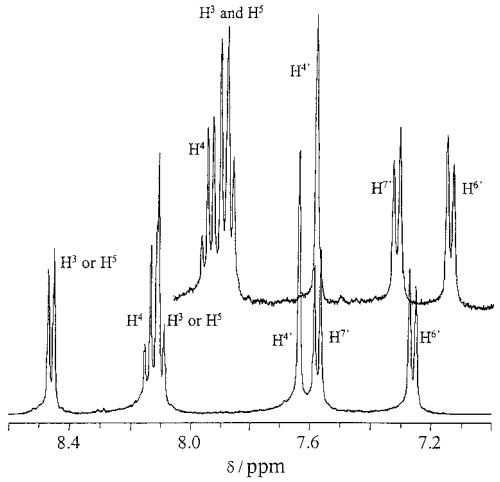

Figure 1. Aromatic region of the ^{1}H NMR spectra of 10^{-2} M L^C in DMSO-d_6 (top) and D_2O at pD = 13.0 (bottom).

under the same experimental conditions confirmed the presence of two different equivalent points as well as the pK_a values. We note that pK_{a1} is intermediate between pK_a = 3.96 ± 0.04 for L^4 (determined under similar experimental conditions: concentration = 7.1 × 10^{-4} M, starting pH = 10.6) and pK_{a1} = 4.63 for dipicolinic acid.[49] On the other hand, the ΔpK_a separation for L^C (3.3 log units) is larger than the one observed for the latter diacid (2.6 log units).[49] Since (i) the two carboxylic groups in L^C are topologically separated by at least 17 atoms and (ii) the methylene bridge in L^C is not a good electronic relay between the two arms of the ligand, the observation of two significantly different pK_a values means that the two arms are either interacting through space or involved in some intermolecular association: the expected statistical separation for two noninteracting groups belonging to the same molecule is ΔpK_a = 0.6.[50] The ES-MS spectrum recorded at pH = 6.7 displays one peak at m/z = 556.6 corresponding to $[2M + H_2O + H]^+$, but dimeric fragments are often observed under these experimental conditions,[44] and ^{1}H NMR spectra measured in the pD range 6.1−13.0 do not bring supporting evidence for the formation of an intermolecular association in dilute solution, so we think that the second pK_a value is most probably due to an intramolecular interaction between the two ligand arms occurring after the first deprotonation (vide infra).

The solution structure of 10^{-2} M L^C in DMSO-d_6 was investigated by ^{1}H and ^{13}C NMR, including {^{1}H−^{1}H} COSY and {^{1}H−^{13}C} HSQC experiments since the diacid is too insoluble to be studied in water (Figure 1; Figure F1, Supporting Information; Table 2). At room temperature, the spectra are typical of a species with a C_{2v} symmetry since (i) only 9 proton and 16 carbon signals are observed for the 26 protons and 31 carbon atoms of L^C and (ii) the two methylene probes display enantiotopic protons. NOE effects are evidenced between the bridging methylene protons and H$^{4'}$, H$^{6'}$ as well as between H$^{7'}$ and the methylene protons of the ethyl substituent, while no such effect is detected between the latter and the aromatic protons of the pyridine unit. This points to a transoid conformation of the two ligand arms, with the *N*-ethyl substituent on the benzimidazole moiety on the same side as the N atom of the pyridine ring (cf. Chart 1). The monoacid L^4 was found to possess the same conformation. Similar arrangements have been observed with tridentate receptors based on bis(benzimidazole)-pyridine units,[43] and this conformation is also predicted by molecular mechanic calculations (Figure 2).

Table 2. ^{1}H and ^{13}C Chemical Shifts (ppm vs TMS) of 10^{-2} M L^C in DMSO-d_6 and 10^{-2} M $[L^C\text{-H}]^-$ and $[L^C\text{-2H}]^{2-}$ in D_2O at 298 K[a]

	CH_2 (br)[e]	CH_2 (Et)	CH_3 (Et)	3 or 5	3 or 5	4	4′	6′	7′
				L^C in DMSO-d_6					
^{1}H, δ/ppm	4.20	4.87	1.38	8.10	8.46	8.14	7.64	7.26	7.58
J/Hz		6.6	6.6	6.1	7. 5	7.5		8.4	8.4
^{13}C, δ/ppm[b]	45.1	44.2	19.1	130.6	128.7	142.5	122.8	128.7	114.5
				$(L^C\text{-H})^-$ in D_2O at pD = 6.1					
^{1}H, δ/ppm	3.85	4.42	1.11	7.86	7.79	7.88	7.49	7.03	7.20
J/Hz		7.0	7.0	7.4	7.0	7.7		8.4	8.4
				$(L^C-2H)^{2-}$ in D_2O at pD = 13.0					
^{1}H, δ/ppm	4.0	4.47	1.14	7.92	7.87	7.92	7.56	7.12	7.30
J/Hz	7.2	7.0	7.0	7.9	8.0	7.9		8.1	8.3
^{13}C, δ/ppm[c]	49.3	41.0	14.2	125.6	124.7	138.4	117.9	124.0	110.8
				L^4; $(L^4\text{-H})^-$ in D_2O at pD = 5.4−13.6 [d]					
^{1}H, δ/ppm		4.73	1.37	8.07	8.07	8.15	7.75	7.50	7.81

[a] The ^{1}H chemical shifts of L^4 and $[L^4\text{-H}]^-$ are also reported for comparison purposes.− [b] Other signals: 170.0 (*C*O), 153.6, 152.2, 151.9, 146.0, 138.5, 140.7 (quat. *C*). [c] Other signals: 172.7 (*C*O), 153.7, 150.1, 147.8, 141.3, 133.5, 130.3, (quat. *C*). [d] The two species display the same spectrum; proton H$^{5'}$appears at 7.45 ppm. [e] Bridge.

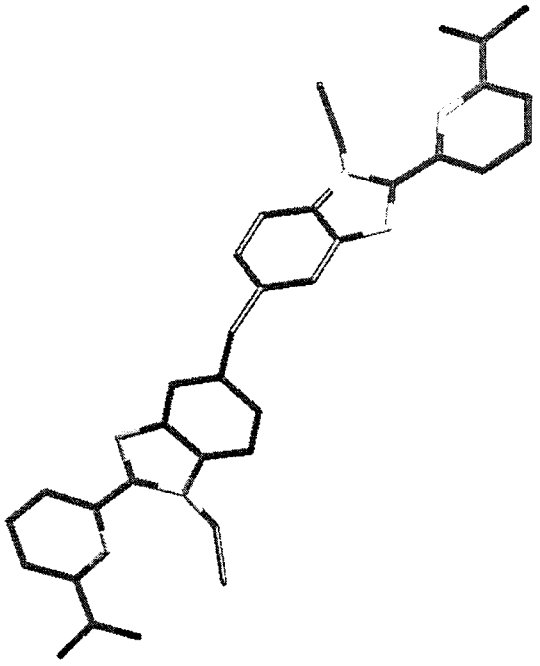

Figure 2. Optimized geometry of ligand L^C.

In D_2O at pD = 13.0, we essentially have the dianion in solution (>99%), and the ^{1}H NMR spectrum is much like that of L^C in DMSO-d_6. NOE effects are also consistent with a transoid conformation for $[L^C\text{-2H}]^{2-}$. At pD = 6.1 (corresponding to the first neutralization), the monodeprotonated form is predominant, and the spectrum is similar to the spectrum of $(L^C\text{-2H})^{2-}$. In contrast, the ^{1}H NMR spectrum of L^4 in D_2O is practically pD-independent between 5.4 (precipitation limit) and 13.6, and we interpret this difference with respect to L^C as being consistent with the assumption of an intramolecular interaction taking place between the carboxylic and the carboxylate functions in $[L^C\text{-H}]^-$ and resulting in a larger than expected pK_{a2} value.

(49) Lewis, M. R.; Deerfield, D. W.; Hoke, R. A.; Koehler, K. A.; Pedersen, L. G.; Hiskey, R. G. *J. Biol. Chem.* **1988**, *263*, 1358.
(50) Perlemutter-Hayman, B. *Acc. Chem. Res.* **1986**, *19*, 90.

Complex Formation in Water. ^{1}H NMR titration of $[L^C\text{-}2H]^{2-}$ with $Eu(ClO_4)_3 \cdot nH_2O$, in D_2O at pD = 12.7, points to the exclusive formation of a 2:3 species with a break at $[Eu]_t/[L^C\text{-}2H]_t = 0.64$ and no hydroxide precipitation before the break point (Figure F2, Supporting Information). This speciation is confirmed by spectrophotometric data obtained at lower pH = 7.2 (Figure F2, Supporting Information) in H_2O ($[L^C\text{-}2H]_t = 1.05 \times 10^{-5}$ M, $0 < [Ln]_t < 1.6 \times 10^{-5}$ M), which could be fitted to eq 1 for Ln = La ($\log \beta_{23} = 30 \pm 1$), Eu ($26.1 \pm 0.4$), and Lu ($27.3 \pm 0.6$). As a comparison, helicates formed by L^B

$$2Ln^{3+} + 3[L^C\text{-}2H]^{2-} \rightleftharpoons [Ln_2(L^C\text{-}2H)_3] \qquad \log \beta_{23} \quad (1)$$

in aprotic CH_3CN display $\log \beta_{23}$ values in the range 24−25.[30] The replacement of the carboxamide functions by carboxylate groups therefore induces a much larger stability for the dimetallic helicates, but the expected values for $\log \beta_{23}$ are beyond the upper limit of what can be reasonably extracted by such a spectrophotometric method at ca. 10^{-5} M, especially when the spectra of the different species in equilibrium are strongly correlated. We have thus performed competitive titration experiments in D_2O ($9.8 < pD < 10.4$) in the presence of 1,4,7,10-tetraazacyclododecane-*N*,*N*′,*N*″,*N*‴-tetraacetic acid (dota). In view of the slow kinetics of formation of the $[Ln(dota)]^-$ complexes,[51] solutions were equilibrated for 5 days at 50 °C and for 1 week at room temperature prior to measurement. The concentrations of the $[Eu_2(L^C)_3]$ helicate and of free L^C were estimated from the ^{1}H NMR signals of the methyl groups of the ethyl substituent of the benzimidazole units. Taking into account $\log K(Eudota^-) = 23.5$,[52] we get $\log \beta_{23}(Eu) = 51 \pm 4$. Although this figure can be taken only as an estimate, it clearly demonstrates that the neutral $[Eu_2(L^C)_3]$ helicate has a stability comparable to that of the dota complex, with a pEu value (for $[Eu]_t = 10^{-6}$ M and $[L]_t = 10^{-5}$ M)[53] around 21, as compared to 25 for dota.

Solid-State Structure of $[Ln_2(L^C\text{-}2H)_3]\cdot 20.5H_2O$ (Ln = Eu, 13a; Tb, 15a). Complexes were isolated for the entire Ln series from DMF solutions in which they are much less soluble than the ligand. Crystallization was carried out in water, and colorless crystals were obtained by slow evaporation of the aqueous solution for Eu and by diffusion of acetone for Tb. The atom-numbering scheme is depicted in Figure 3, selected bond lengths are reported in Table 3, and a stereoview of the Tb complex is shown in Figure 4. Atomic coordinates, anisotropic displacement parameters, and selected angles are reported in Tables S3−S5 (Supporting Information). In agreement with vibrational and elemental analyses, crystallographic data show that both compounds crystallize without perchlorate anions. The asymmetric units are comprised of two slightly different neutral dimetallic helicates, in which the coordination environment of the Ln^{III} ion consists exclusively of the three oxygen and six nitrogen donor atoms from the three ligand strands. $Ln^{III}-Ln^{III}$ distances are longer in molecules B (9.04−9.07 Å) than in molecules A (8.81−8.82 Å). They correspond to the distances measured in the dimetallic helicates $[Tb_2(L^B)_3]^{6+}$ (9.06 Å)[30] and $[Eu_2(L^A)_3]^{6+}$ (8.88 Å).[54] In view of the experimental conditions used, partial protonation of one or several ligand strands cannot be completely ruled out; we have therefore carefully examined the carbonyl

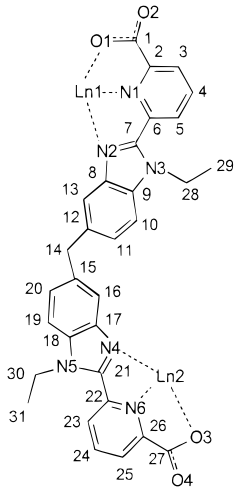

Figure 3. Atom-numbering scheme for the first ligand strand in $[Ln_2(L^C\text{-}2H)_3]\cdot 20.5H_2O$ (Ln = Eu, **13a**; Tb, **15a**). The numbering of the other ligand strands starts at O5, N7, and C32, and O9, N13, and C63, respectively.

C−O distances (Table S6, Supporting Information) and compared them to data for a Gd^{III} oxidiacetate complex, featuring coordination to both carboxylate and carboxylic moieties,[55] to $[Tb(teta)]^-$,[56] to $[Eu(dota)]^-$,[57] and to two tris(dipicolinate) complexes.[58] Experimental C−O bond lengths are alike, despite the diversity of the compounds used for comparison, and the mean C−O distances found in our compounds are in agreement with the coordination of the metal ion to carboxylate groups.

The coordination polyhedra of the Ln^{III} ions in both molecules A and B can be described as distorted tricapped trigonal prisms which are considered to be comprised of three tripods: O atoms from the carboxylates define the upper tripod, N atoms from the benzimidazole moieties delineate the lower tripod, and the N atoms from the pyridine rings represent the capping tripod (Figure 5). The average Ln−O and Ln−N distances are listed in Table 4, along with comparison data. The mean Ln−O distances for the four coordination sites are homogeneous and intermediate between those found in dipicolinate and dota complexes. However, the mean Tb−O distance is shorter by 0.05 Å than in $[Tb(L^2\text{-}2H)_3]^{3-}$,[59] while the Eu−O distance is longer than in $[Eu(L^2\text{-}2H)_3]^{3-}$ [58] and corresponds to the distance found in $[Eu(L^3)_3]^{3+}$.[60] In helicates with L^A and L^B and in triple helical complexes with L^1, the mean Ln−N(benzimidazole) and Ln−N(pyridine) distances are almost equal, which is not the case for $[Ln_2(L^C\text{-}2H)_3]$, where the mean Ln−N(benzimidazole) bond lengths are longer than the mean Ln−N(pyridine) bond lengths, as a result of the strong carboxylate coordination. In the two structures, the metal ions are located on a pseudo-C_3 axis, and three pseudo-C_2 axes going through the bridging methylene group of each ligand strand lead to a pseudo-D_3 symmetry of the triple-stranded dimetallic helicates. In the Eu^{III} helicate with L^C, there is a difference between molecules A and B (Tables S7−S11, Supporting Information): the dihedral angles between the connected pyridine and benzimidazole rings

(51) Burai, L.; Fabian, I.; Kiraly, R.; Szilagyi, E.; Brucher, E. *J. Chem. Soc., Dalton Trans.* **1998**, 243.
(52) Cacheris, W. P.; Nickle, S. K.; Sherry, A. D. *Inorg. Chem.* **1987**, *26*, 958.
(53) Vögtle, F. *Supramolecular Chemistry;* John Wiley: Chichester, 1991.
(54) Piguet, C.; Bünzli, J.-C. G.; Bernardinelli, G.; Hopfgartner, G.; Williams, A. F. *J. Alloys Compd.* **1995**, *225*, 324.
(55) Baggio, R.; Garland, M. T.; Perec, M. *Inorg. Chem.* **1997**, *36*, 950.
(56) Spirlet, M. R.; Rebizant, J.; Loncin, M. F.; Desreux, J. F. *Inorg. Chem.* **1984**, *23*, 4278.
(57) Spirlet, M. R.; Rebizant, J.; Desreux, J. F.; Loncin, M. F. *Inorg. Chem.* **1984**, *23*, 359.
(58) Brayshaw, P. A.; Bünzli, J.-C. G.; Froidevaux, P.; Harrowfield, J. M.; Kim, Y.; Sobolev, A. N. *Inorg. Chem.* **1995**, *34*, 2068.
(59) Hu, S.; Dong, Z.; Zhang, H.; Liu, Q. *Xiamen Daxue Xuebao, Ziran Kexue* **1989**, *28*, 279.
(60) Renaud, F.; Piguet, C.; Bernardinelli, G.; Bünzli, J.-C. G.; Hopfgartner, G. *Chem. Eur. J.* **1997**, *3*, 1646.

Table 3. Selected Bond Lengths (Å) in $[Ln_2(L^C\text{-}2H)_3]\cdot 20.5H_2O$[a]

molecule A	Ln = Eu	Ln = Tb	molecule B	Ln = Eu	Ln = Tb
Ln(1A)−O(1A)	2.379(6)	2.340(4)	Ln(1B)−O(1B)	2.337(5)	2.317(3)
Ln(1A)−O(5A)	2.408(6)	2.369(4)	Ln(1B)−O(5B)	2.447(6)	2.413(4)
Ln(1A)−O(9A)	2.422(7)	2.389(4)	Ln(1B)−O(9B)	2.421(7)	2.383(4)
Ln(1A)−N(1A)	2.569(7)	2.549(5)	Ln(1B)−N(1B)	2.558(7)	2.510(5)
Ln(1A)−N(2A)	2.604(8)	2.596(5)	Ln(1B)−N(2B)	2.627(7)	2.620(5)
Ln(1A)−N(7A)	2.548(7)	2.544(4)	Ln(1B)−N(7B)	2.583(7)	2.564(4)
Ln(1A)−N(8A)	2.634(7)	2.588(5)	Ln(1B)−N(8B)	2.620(7)	2.600(4)
Ln(1A)−N(13A)	2.594(7)	2.567(5)	Ln(1B)−N(13B)	2.562(7)	2.547(4)
Ln(1A)−N(14A)	2.620(7)	2.601(4)	Ln(1B)−N(14B)	2.632(7)	2.620(5)
Ln(2A)−O(3A)	2.372(6)	2.353(3)	Ln(2B)−O(3B)	2.395(6)	2.362(4)
Ln(2A)−O(7A)	2.378(7)	2.355(4)	Ln(2B)−O(7B)	2.398(7)	2.372(4)
Ln(2A)−O(11A)	2.404(6)	2.366(4)	Ln(2B)−O(11B)	2.466(6)	2.424(4)
Ln(2A)−N(4A)	2.662(7)	2.632(5)	Ln(2B)−N(4B)	2.581(8)	2.552(5)
Ln(2A)−N(6A)	2.615(7)	2.580(5)	Ln(2B)−N(6B)	2.549(7)	2.516(4)
Ln(2A)−N(10A)	2.616(7)	2.608(5)	Ln(2B)−N(10B)	2.624(7)	2.619(5)
Ln(2A)−N(12A)	2.567(7)	2.543(5)	Ln(2B)−N(12B)	2.554(7)	2.520(5)
Ln(2A)−N(16A)	2.652(6)	2.622(4)	Ln(2B)−N(16B)	2.665(6)	2.640(4)
Ln(2A)−N(18A)	2.578(7)	2.556(4)	Ln(2B)−N(18B)	2.543(7)	2.511(4)
Ln(1A)···Ln(2A)	8.807(3)	8.829(1)	Ln(1B)···Ln(2B)	9.044(3)	9.069(1)

[a] Standard deviations are indicated between parentheses.

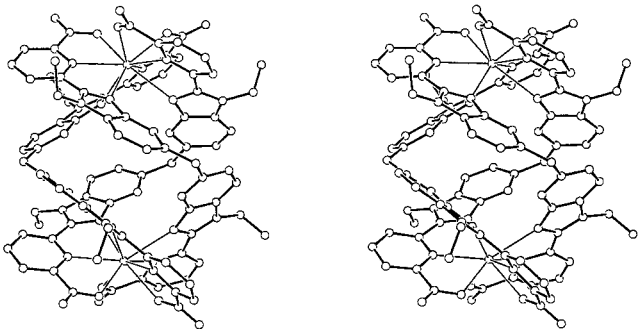

Figure 4. Stereoview of molecule A in $[Tb_2(L^C\text{-}2H)_3]\cdot 20.5H_2O$ (**15a**).

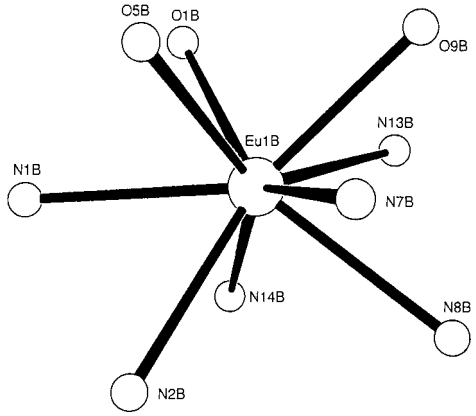

Figure 5. ORTEP representation of the coordination polyhedron around Eu1B in $[Eu_2(L^C\text{-}2H)_3]\cdot 20.5H_2O$ (**13a**).

range between 9.6 and 28.3° (mean value 22.2°) in molecule A and between 17.6 and 38.6° (mean value 26.0°) in molecule B. A comparable situation holds for the dimetallic Tb^{III} edifices, with mean values of 22.0 (A) and 25.5° (B). As a comparison, these twist angles range between 9.8 and 27.3° (mean value 23°) in $[Eu_2(L^A)_3]^{6+}$ [29] and between 8.9 and 31.3° (mean value 22.4°) in $[Tb_2(L^B)_3]^{6+}$.[30] The dihedral angles between the benzimidazole groups belonging to two different ligand strands range between 14.8 and 21° (Eu) and between 10.9 and 26.9° (Tb), while the associated contact distances between these planes are larger than 3.95 Å, which precludes the existence of sizable interstrand $\pi-\pi$ stacking interactions similar to those observed in $[Eu(L^1)_3]^{3+}$ (3.1−3.3 Å, mean angle 9.1°).[16] A closer examination of the dihedral angles between the connected benzimidazole moieties of the same ligand strand reveals that molecule B is more distorted.

Table 4. Average Ln−O and Ln−N Distances (Å) in the $[Ln_2(L^C\text{-}2H)_3]$ (Ln = Eu, Tb) Helicates and in Related Compounds

compound		Ln−N benzimidazole	Ln−N pyridine	Ln−O	ref
$[Eu(L^1)_3]^{3+}$		2.60	2.58		16
$[EuZn(L^{II})_3]^{5+}$		2.57	2.60	2.38	21
$Cs_3[Eu(L^2\text{-}2H)_3]$			2.53	2.48	58
$[Eu(dota)]^-$				2.39	57
$[Eu_2(L^A)_3]^{6+}$	Eu1	2.57	2.60		29
	Eu2	2.61	2.60		
$[Eu_2(L^C-2H)_3]$	Eu1A	2.62	2.57	2.40	this work
	Eu2A	2.64	2.59	2.39	
	Eu1B	2.63	2.57	2.40	
	Eu2B	2.62	2.55	2.42	
$[Tb_2(L^B)_3]^{6+}$	Tb1	2.56	2.57	2.36	30
	Tb2	2.59	2.59	2.36	
$[Tb(L^2\text{-}2H)_3]^{3-}$			2.51	2.42	59
$[Tb(teta)]^-$				2.32	56
$[Tb_2(L^C-2H)_3]$	Tb1A	2.60	2.55	2.37	this work
	Tb2A	2.62	2.56	2.36	
	Tb1B	2.61	2.54	2.37	
	Tb2B	2.60	2.52	2.39	

A dimetallic helical edifice is characterized by its pitch,[31] which is the distance necessary for the ligand to achieve a 360° rotation. The pitch (P) in $[Ln_2(L^C\text{-}2H)_3]$ can be estimated from the N(py)−Ln1−Ln2−N(py) dihedral angles (α) and the intramolecular intermetallic distance (d) according to $P = d/(\alpha/360)$,[61,62] since the N(py)−Ln1−Ln2 angles are close to 90°. We calculate P = 23.7 (A) and 24.5 Å (B) for the Eu^{III} helicates and P = 23.8 (A) and 24.7 Å (B) for the Tb^{III} edifices. The wrapping of the three ligand strands $[L^C\text{-}2H]^{2-}$ around the two lanthanide ions is not too different from what is observed with ligands L^A and L^B, whose helicates have pitches equal to 25.0 and 24.0 Å, respectively.

The degree of distortion of the tricapped trigonal prisms has been investigated quantitatively using a geometric analysis based on the determination of three angles, ϕ, θ_i, and ω_i (Figure 6).[17] The average bending of the upper (vs(j)) and lower (vi(j)) tripods is measured by the angle ϕ between the sum vectors $\mathbf{R}_1$ and $\mathbf{R}_2$

(61) Renaud, F.; Piguet, C.; Bernardinelli, G.; Hopfgartner, G.; Bünzli, J.-C. G. *Chem. Commun.* **1999**, 457.
(62) Renaud, F.; Piguet, C.; Bernardinelli, G.; Bünzli, J.-C. G.; Hopfgartner, G. *J. Am. Chem. Soc.* **1999**, *121*, 9326.

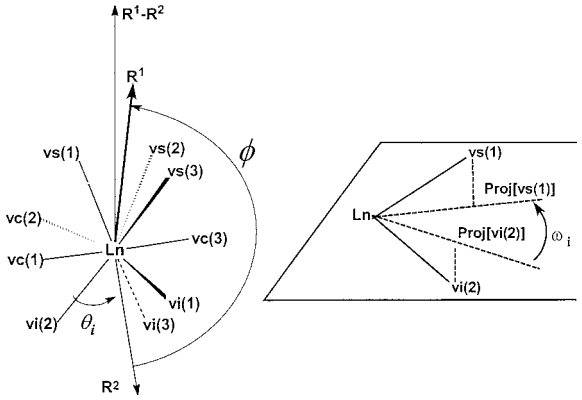

Figure 6. Definition of the angles and vectors used in the analysis of the coordination polyhedra.

Table 5. Geometric Analysis of the Coordination Polyhedra in $[Ln_2(L^C\text{-}2H)_3]\cdot 20.5H_2O$ (Ln = Eu, **13a**; Tb, **15a**) and in Related Compounds

compound		α/deg[a]	*d*/Å[b]	*ϕ*/deg	mean *θ* vs_i-R^1/deg	mean *θ* vi_i-R^2/deg	ref
$[Eu(L^1)_3]^{3+}$		0	3.25	179.9	51.0	51.7	16
$[Co(sar)][Eu(L^2\text{-}2H)_3]$		2.3	3.33	179.1	46.7	47.4	58
$[EuZn(L^{II})_3]^{5+}$		2.0	3.16	179.0	47.7	48.0	21
$[Eu(L^3)_3]^{3+}$		3.5	3.26	178	47.5	52.8	60
$[Eu_2(L^A)_3]^{6+}$	site 1	3.2	3.22	178.0	51.5	51.2	29
	site 2	2.9	3.24	179.0	51.4	51.6	
$[Eu_2(L^C-2H)_3]$	site 1A	3.1	3.16	178.6	50.5	51.2	*c*
	site 2A	3.8	3.16	179.6	49.6	52.5	
	site 1B	6.1	3.23	178.0	49.0	50.8	
	site 2B	7.4	3.23	178.4	51.0	49.2	
$[Tb(L^2\text{-}2H)_3]^{3-}$		5.4	3.35	179.2	45.3	47.1	59
$[Tb_2(L^B)_3]^{6+}$	site 1	1.5	3.15	177.6	47.5	52.5	30
	site 2	2.1	3.16	178.5	48.8	51.6	
$[Tb_2(L^C\text{-}2H)_3]$	site 1A	2.9	3.14	178.9	50.6	51.1	*c*
	site 2A	3.1	3.13	179.4	49.4	52.4	
	site 1B	6.2	3.21	178.0	48.9	50.6	
	site 2B	7.8	3.22	178.0	50.6	49.2	

[a] Angle between the facial planes of the distal tripods. [b] Distance between the facial planes of the distal tripods. [c] This work.

($\mathbf{R}_1 = \sum_{j=1}^{3} \mathrm{Ln} - \mathrm{vs}(j)$, $\mathbf{R}_2 = \sum_{j=1}^{3} \mathrm{Ln} - \mathrm{vi}(j)$, and $\phi = 180°$ for an ideal trigonal prism), while the angles θ_i reflect the flattening of the coordination polyhedron along the pseudo-C_3 axis, defined as $\mathbf{R}_2 - \mathbf{R}_1$. Finally, the angles ω_i show the deformation of the distal tripods from the trigonal prism (ideal value 0°) toward an octahedron (ideal value 60°). In both Eu^{III} and Tb^{III} helicates, the ϕ angles range between 177.6 and 179.6° and do not deviate significantly from the expected value for a perfect trigonal prism, indicating a small bending of the two distal tripods. This is confirmed by the almost parallel arrangement of the facial planes, as shown in Table 5 (cf. also Tables S12 and S13, Supporting Information) for the two investigated helicates and for related compounds; we note, however, that the interplanar angle α is larger for molecules B (6.1−7.8°) than for molecules A (2.9−3.8°). Analysis of the θ_i angles reported in Table 5 (cf. also Table S14, Supporting Information) discloses that individual values do not deviate much from their mean values, which are in the range 49.4−52.5° for molecules A and 49.0−51.0° for molecules B, with a largest deviation of 3.5°, pointing to slightly distorted polyhedra. The flattening of the polyhedron along the pseudo-C_3 axis is somewhat more important in molecules A than in molecules B, in line with the longer $Ln^{III}-Ln^{III}$ distance observed in the latter. The angles ω_i between projection vectors of the two distal tripods (7.1−13.5°, Table S15, Supporting Information) are relatively close to the expected value of 0° for an ideal trigonal prism.

One of the most important features of the structures is the presence of an extensive network of 41 water molecules per asymmetric unit, 23 of them interacting with carboxylate groups (Figure 7; Table S16, Supporting Information). The carboxylate groups of sites 1A interact with seven water molecules and those of sites 2B with six, while sites 1B and 2A also interact with respectively seven and six molecules, but three of them are shared and provide a link between one A and two B molecules in the same unit cell. As a result, the intermolecular Ln2A−Ln1B distance is 15.2 Å, as compared to 18.0 Å for the Ln1A−Ln2B distance. Noticeable differences in the H-bonding interactions appear between molecules A and B. For instance, one of the carboxylate function of site 1B (O1B) does not interact with any water molecule, which induces the shortest Ln−O distance (2.34 Å for Eu, 2.31 Å for Tb). On the other hand, the carboxylate groups which are the more involved in H-bonding (O5B, O6B, four H-bonds; O9B, O10B, three H-bonds) correspond to the longest Ln−O distances. Therefore, it appears that subtle interactions arising from the extensive H-bond network surrounding the supramolecular edifices are responsible for the differences observed between molecules A and B, in particular the longer Ln1B−Ln2B distances compared to Ln1A−Ln2A.

Solution Structure of $[Ln_2(L^C\text{-}2H)_3]$ in D_2O. ^1H NMR spectra have been recorded at pD's between 7.4 and 8.5, depending upon the Ln^{III} ion. The spectra (Table 6) display only nine signals for the three ligand strands, pointing to a ternary symmetry. The bridging CH_2 group shows an A_2 spin system, which is typical for two C_2-related enantiotopic protons, while the *AB* spin system observed for the other methylene group arises from two symmetrically nonequivalent diastereotopic protons, leading to the conclusion that the helicates adopt time-averaged D_3 symmetry on the NMR time scale.[29] Analysis of the spectra for the edifices with diamagnetic Ln^{III} ions (La, Y, Lu) reveals that the ionic radius contraction does not modify substantially the overall structure of the helicates. However, the signal of the $H^{4'}$ proton is shifted on going from La to Y ($\Delta\delta = +0.47$ ppm) and Lu (+0.59 ppm), pointing to some distortion in the coordination sphere of the metal ions. The large shift experienced by this proton upon complexation (+1.21 ppm for La) can be traced back to the peculiar conformation of the diphenylmethylene spacing moiety, which puts $H^{4'}$ in the shielding zone of the adjacent benzimidazole moieties.[29] The pyridine protons also undergo substantial shifts upon complexation, reflecting the coordination of the N atom of the pyridine to the metal ions with concomitant change from a transoid to a cisoid arrangement of the two arms of the ligand, the *N*-ethyl substituent on the benzimidazole moiety lying now on the opposite side of the N atom of the pyridine ring, as demonstrated by NOE effects detected between CH_2(ethyl) and H^3.

For axial paramagnetic monometallic lanthanide complexes, finer structural information can be gained from the separation of contact (δ_{ij}^{c}) and pseudocontact (δ_{ij}^{pc}) contributions to the isotropic paramagnetic shift δ_{ij}^{para}.[63,64] The experimental shift δ_{ij}^{exp} for a nucleus *i* in an axial complex of lanthanide *j* is the

(63) Sherry, A. D.; Geraldes, C. F. G. C. In *Lanthanide Probes in Life, Chemical and Earth Sciences. Theory and Practice*; Bünzli, J.-C. G., Choppin, G. R., Eds.; Elsevier Science Publ. B.V.: Amsterdam, 1989.

(64) Bertini, I.; Luchinat, C. *NMR of Paramagnetic Molecules in Biological Systems*; The Benjamin/Cummings Publ. Co. Inc.: Menlo Park, CA, 1986.

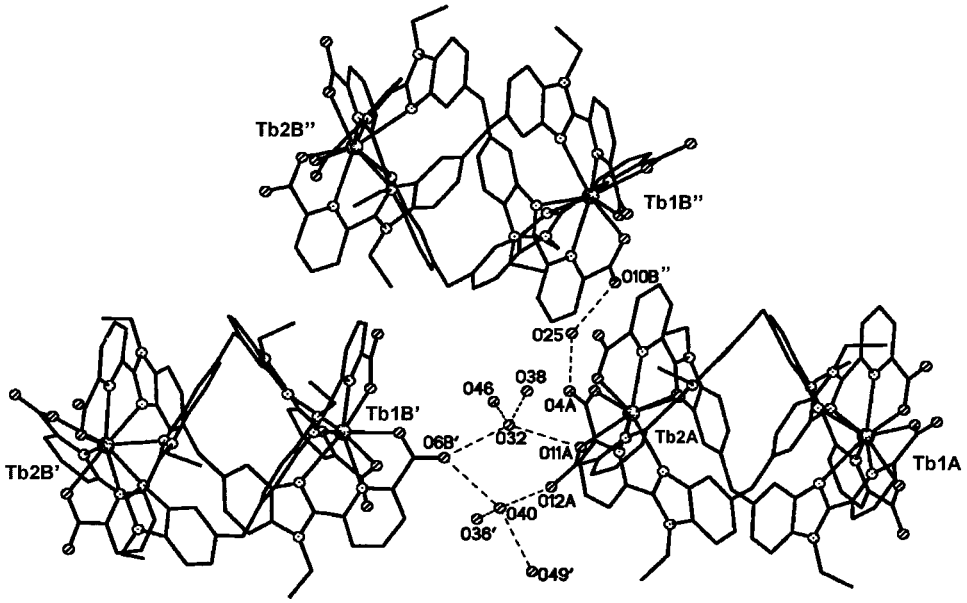

Figure 7. Water molecules in $[Ln_2(L^C\text{-}2H)_3]\cdot 20.5H_2O$ (Ln = Eu, **13a**; Tb, **15a**) interacting with both A and B molecules. Primed numbers indicate atoms generated by symmetry operations.

Table 6. ^{1}H NMR Shifts (ppm vs TMS) for $[Ln_2(L^C\text{-}2H)_3]$ Solutions 10^{-2} M in D_2O ($7.4 < pD < 8.5$)

	b-CH_2	CH_2 (ethyl)	CH_3 (ethyl)	3	4	5	4′	6′	7′
La	3.46	4.48	1.38	8.16	7.95	7.39	6.24	7.09	7.34
Y	3.45	4.55	1.37	8.19	7.90	7.40	5.77	7.05	7.33
Lu	3.46	4.59	1.37	8.20	7.86	7.38	5.65	7.03	7.32
Ce	2.92	6.14	3.21	10.71	10.23	10.06	−0.53	6.93	7.81
Pr	2.55	7.49	4.51	13.01	11.86	12.15	−6.02	6.81	8.34
Nd	2.91	6.13	3.06	11.58	10.36	10.36	−6.52	6.91	8.15
Sm	3.30	4.92	1.78	8.63	8.35	7.95	2.65	6.98	7.32
Eu	4.30	2.64	−0.80	3.05	4.80	2.97	22.1	7.38	6.03
Tb	−4.07	37.15	27.51	31.71	27.51	23.51	1.49	3.10	7.19
Er	5.42	0.28	−3.99	2.13	0.43	0.85	43.5	5.85	8.11
Tm	8.84	−7.69	−14.13	−11.86	−8.14	−13.84	99.02	5.75	10.14
Yb	5.50	0.13	−4.23	1.25	2.20	0.25	46.11	6.94	8.29

sum of three contributions,

$$\delta_{ij}^{exp} = \delta_{ij}^{para} + \delta_i^{dia} + \delta_j^{bulk} \quad (2)$$

δ_j^{bulk} cancels out when using an internal reference, and δ_i^{dia} is obtained by measuring chemical shifts for isostructural diamagnetic complexes:[61,62,63] we have used $[La_2(L^C\text{-}2H)_3]$ for Ln = Ce−Nd, $[Y_2(L^C\text{-}2H)_3]$ for Sm−Tb, and $[Lu_2(L^C\text{-}2H)_3]$ for Ho−Yb. The isotropic lanthanide-induced paramagnetic shift (LIS) is given by eq 3, but the existence of two identical paramagnetic centers in the homodimetallic helicates $[Ln_2(L^C\text{-}2H)_3]$ requires some modifications of the classical equations derived for monometallic complexes:[63,64]

$$\delta_{ij}^{para} = \delta_{ij}^{exp} - \delta_i^{dia} = \delta_{ij}^{c} + \delta_{ij}^{pc} \quad (3)$$

Since (i) no magnetic coupling occurs at room temperature between Ln^{III} ions lying at distances larger than 4 Å[63,65] and (ii) the aromatic tridentate binding units are separated by methylene bridges in L^C which are poor electronic relays, we assume that the contact contributions δ_{ij}^c result from through-bond Fermi interactions with a single metallic center and are given by eq 4, where A_i is the hyperfine coupling constant between the electronic spin of the Ln_j^{III} and the magnetic moment of the nucleus i, B_0 is the applied magnetic induction, $\langle S_z\rangle_j$ is the spin expectation value of S_z for a single metallic site, and F_i is the contact term at a fixed temperature. On the other hand, pseudocontact contributions resulting from through-space effects affect paramagnetic shifts for protons which are significantly remote from the paramagnetic center,[63] and the contributions of both metallic centers must be considered for the nucleus i. Taking into account the geometrical arrangement shown in Scheme 3, where the metal ion is located at the origin, and the reasonable hypothesis[66] that the deviation of the z axis of the magnetic susceptibilty tensor from the molecular axis is negligible for lanthanide complexes having at least 3-fold symmetry, we obtain[63]

$$\delta_{ij}^{c} = \frac{A_i\langle S_z\rangle_j}{\hbar\gamma B_0 T} = F_i\langle S_z\rangle_j \quad (4)$$

$$\delta_{ij}^{pc} = \sum_{n=1}^{2}\frac{k_{CF}^n}{T^2}\left(\frac{1-3\cos^2\theta_i^n}{(r_i^n)^3}\right)C_j^n = \sum_{n=1}^{2} G_i^n C_j^n \quad (5)$$

k_{CF}^n is the crystal field parameter, C_j^n is the anisotropic part of the axial magnetic susceptibility tensor, r_i^n and θ_i^n are the internal axial coordinates of nucleus i with respect to the ligand field axis of site n, and G_i^n is the pseudocontact term originating from metal n at a given temperature. For the D_3-symmetrical

(65) Costes, J. P.; Dahan, F.; Dupuis, A.; Lagrave, S.; Laurent, J. P. *Inorg. Chem.* **1998**, *37*, 153.

(66) Kemple, M. D.; Ray, B. D.; Lipkowitz, K. B.; Prendergast, F. G.; Rao, B. N. D. *J. Am. Chem. Soc.* **1988**, *110*, 8275.

Scheme 3

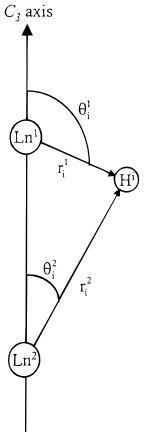

complexes $[Ln_2(L^C\text{-}2H)_3]$, with the two noninteracting paramagnetic Ln^{III} ions separated by ca. 9 Å, $k_{CF}^1 = k_{CF}^2 = k_{CF}$, and we can reasonably approximate $C_j^1 = C_j^2 \approx C_j$. The isotropic paramagnetic shift for the homodimetallic helicates $[Ln_2(L^C\text{-}2H)_3]$ is thus given by the following simplified equation:

$$\delta_{ij}^{para} = \delta_{ij}^{exp} - \delta_i^{dia} = F_i\langle S_z\rangle_j + (G_i^1 + G_i^2)C_j \qquad (6)$$

If we assume that $\langle S_z\rangle_j$ and C_j values are the same for the complexes and the free ions (for which they are tabulated),[63,67] a multilinear least-squares fit of eq 6 for an isostructural series of complexes according to Reilley's method[68] leads to the determination of the contact term F_i and the sum of the two pseudocontact terms $G_i^{global} = G_i^1 + G_i^2$. These calculations require a correct assignment of the various resonances. To secure our assignments, we have used homonuclear $\{^1H-^1H\}$ COSY, $\{^1H-^1H\}$ ROESY, and NOEDIF experiments as well as the program SHIFT ANALYSIS 3.0 developed by Forsberg.[69] The isostructurality of the complexes can be checked by eqs 7, which are two linearized forms of eq 6:

$$\frac{\delta_{ij}^{para}}{\langle S_z\rangle_j} = F_i + G_i^{global}\frac{C_j}{\langle S_z\rangle_j} \quad \text{and} \quad \frac{\delta_{ij}^{para}}{C_j} = G_i^{global} + F_i\frac{\langle S_z\rangle_j}{C_j} \qquad (7)$$

We have not used $[Sm_2(L^C\text{-}2H)_3]$ in our calculation because the shifts induced by Sm^{III} are small and extremely temperature-dependent. The diastereotopic methylene protons of the ethyl substituent have also been excluded because a reliable assignment is not possible for an *AB* spin system.[20] Plots according to eqs 7 tend to demonstrate that the helicates with the heavier Ln^{III} ions are not isostructural with the edifices containing the lighter ions (Figure 8; Figure F4, Supporting Information): a first isostructural series encompasses Ce−Tb, while Er−Yb gives another straight line. Care must, however, be exercised in interpreting such data since a shortening of the Ln−ligand distance upon increasing Z or a change in the nonaxial contribution, or both, could also explain some break in the linear correlation. Computed values of F_i, G_i^{global}, and the agreement factors AF_i and AF_j (eqs 8) are given in Table 7, while δ_{ij}^c and δ_{ij}^{pc} data are listed in Table S17 (Supporting Information). The

$$AF_i = [\sum_j(\delta_{ij}^{exp} - \delta_{ij}^{cal})^2/\sum_j(\delta_{ij}^{exp})^2]^{1/2} \quad \text{and}$$

$$AF_j = [\sum_i(\delta_{ij}^{exp} - \delta_{ij}^{cal})^2/\sum_i(\delta_{ij}^{exp})^2]^{1/2} \qquad (8)$$

agreement factors calculated for both series, $0.025 < AF_i < 0.352$ (Ce−Tb) or $0.002 < AF_i < 0.20$ (Er−Yb), are comparable to those found for 3d−4f helicates $[ZnLn(L)_3]^{5+}$, with L = L^I (0.08−0.27)[20] or L^{II} (0.07−0.20),[21] for $[Ln(L^2\text{-}2H)_3]^{3-}$ (0.04−0.27),[68] or for $[Ln(L^3)_3]^{3+}$ (0.01−0.49).[60] Contact contributions are negligible for spin delocalization at distances longer than five chemical bonds, leading to significant F_i values only for $H^{4'}$, H^3, and H^5 (three bonds) and H^4 (four bonds). We could not determine whether the apparent structural change observed between Tb and Er is gradual or not since the nuclear relaxation induced by Dy^{III} and Ho^{III} leads to broad signals and prevents a clear-cut assignment of the resonances. The large F_i values calculated for the H^3, H^4, and H^5 protons in both structural series point to an important spin density delocalization onto the pyridine ring, as demonstrated previously for $[LnZn(L)_3]^{5+}$, with L = L^I (0.34, 0.18, 0.34)[20] or L^{II} (0.35, 0.17, 0.22).[21] The F_i value obtained for $H^{4'}$ is much larger than the ones observed for the ZnLn helicates, suggesting a larger spin delocalization onto the distal benzimidazole moieties in $[Ln_2(L^C\text{-}2H)_3]$.

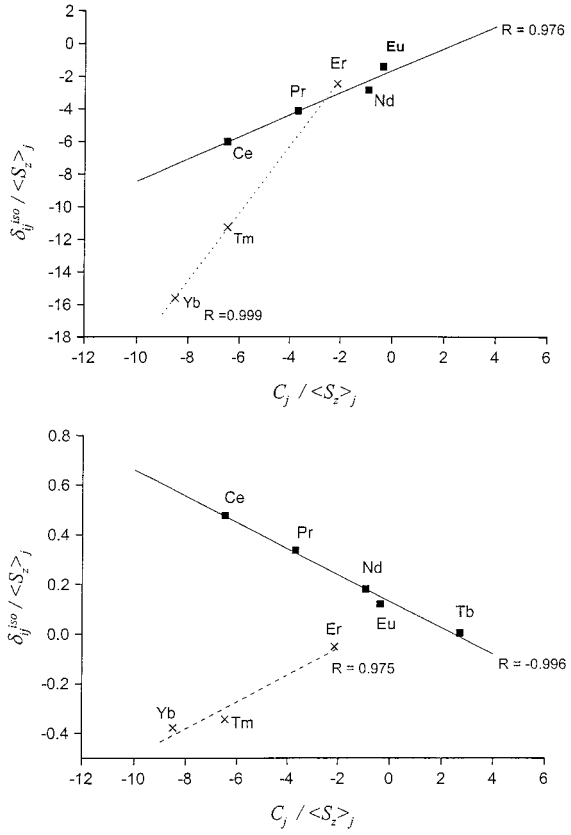

Figure 8. Plots of $\delta_{ij}^{para}/\langle S_z\rangle_j$ vs $C_j/\langle S_z\rangle_j$ for $H^{4'}$ (top) and $H^{7'}$ (bottom) in 10^{-2} M $[Ln_2(L^C\text{-}2H)_3]$ in D_2O at 298 K.

The pseudocontact terms depend on r_i^n and θ_i^n ($n = 1, 2$) and are difficult to interpret because they reflect the sum of two dipolar terms (eqs 5 and 6). However, the $(r_i^n)^{-3}$ dependence limits the contribution of the second metallic site for H^{3-5}. We estimate from the X-ray crystal structure of $[Eu_2(L^C\text{-}2H)_3]$ that the absolute ratios $G^2(H^i)/G^1(H^i)$ ($i = 3-5$) are small and amount to 0.18−0.23, thus leading to the rough approximation that $G^1(H^i) \approx G^{global}(H^i)$ for these protons (Table S17, Supporting Information). According to eq 5, $G^1(H^i)$ will be therefore close to 0 when θ_i^1 tends to 54.7°, and we note that $G^1(H^{3-5})$ have significant negative values, in agreement with their approximate perpendicular orientation with respect to the C_3

(67) Golding, R.; Halton, M. P. *Aust. J. Chem.* **1972**, *25*, 2577.
(68) Reilley, C. N.; Good, B. W.; Desreux, J. F. *Anal. Chem.* **1975**, *47*, 2110.

Table 7. Computed Values for Contact (F_i) and Pseudocontact (G_i^{global}) Terms and Agreement Factors AF_i and AF_j for ^{1}H Nuclei in $[Ln_2(L^C\text{-}2H)_3]$ Solutions 10^{-2} M in D_2O ($7.4 < pD < 8.5$)[a]

	$H^{4'}$	$H^{6'}$	$H^{7'}$	H^3	H^4	H^5	b-CH_2
			Ce−Tb				
θ_i^1/deg	139.85	127.25	120	100.60	88.18	75.49	124.68
r_i^1/Å	3.90	7.27	6.82	5.55	6.27	5.42	6.53
θ_i^2/deg	23.38	52.72	47.59	34.96	34.80	27.27	46.52
r_i^2/Å	6.35	7.27	8.00	9.50	10.96	11.43	7.40
F_i[b]	−1.7(2)	0.011(2)	0.13(1)	0.32(4)	0.21(4)	0.36(5)	−0.02(1)
G_i^{global} [b]	0.76(7)	0.032(8)	−0.05(3)	−0.38(3)	−0.32(1)	−0.35(2)	0.086(4)
AF_i[b]	0.352	0.063	0.038	0.025	0.039	0.083	0.107
F_i[c]	1.193	0	0	0.268	0.229	0.282	0
G_i^{global} [c]	2.348	0.066	−0.009	−0.531	−0.411	−0.528	0.118
AF_i[c]	0.000	0.033	0.137	0.000	0.000	0.000	0.020
			Er−Yb				
F_i[a]	1.99(2)	0.07(5)	0.07(3)	−0.47(2)	−0.15(3)	−0.46(2)	−0.11(4)
G_i^{global} [b]	2.07(4)	−0.004(9)	0.058(9)	−0.41(6)	−0.30(4)	−0.42(7)	0.11(1)
AF_i[b]	0.0015	0.037	0.081	0.198	0.178	0.190	0.055
F_i[c]	0.366	0	0	−0.386	−0.244	−0.388	0
G_i^{global} [c]	1.645	0.046	−0.007	−0.360	−0.288	−0.370	0.083
AF_i[c]	0.000	0.068	0.084	0.000	0.000	0.000	0.086

	Ce	Pr	Nd	Eu	Tb	Er	Tm	Yb
AF_j[b]	0.0174	0.0522	0.0822	0.2091	0.1274	0.0055	0.0365	0.0291
AF_j[c]	0.0120	0.0071	0.0041	0.0038	0.0058	0.0007	0.0001	0.0001

[a] Axial coordinates r_i^n and θ_i^n are tabulated from the X-ray structure of the Eu helicate. [b] According to Reilley's method. [c] According to Kemple's method.

axis ($75.5° < \theta_{3-5}^1 < 100.6°$ in the crystal structure of $[Eu_2(L^C\text{-}2H)_3]$). The absolute $G^1(H^{3-5})$ values tend to be larger for the Er−Yb series than for the lighter Ln^{III} ions, in line with a more compact arrangement and a probable elongation of the helix along the C_3 axis. For $H^{4'}$, $H^{6'}$, and $H^{7'}$, the expected absolute $G^2(H^i)/G^1(H^i)$ ratios are close to 1.0 (0.47−1.01), which precludes a simple access to structural parameters.

Photophysical Properties of the Ligand. In methanol, ligand L^C displays three main absorption bands around 47 540, 40 000, and 31 670 cm^{-1}, which compare well with the absorptions reported for L^B in acetonitrile[30] (Table S18, Figure F5, Supporting Information). The high-energy band is the more intense, is blue-shifted with respect to the corresponding transition for L^B (43 670 cm^{-1}), and is assigned to the $\pi\rightarrow\pi^*$(C=O) transition. The second and third absorptions arise from the pyridine and benzimidazole moieties (41 322 and 32 200 cm^{-1} for L^B).[30] The absorption spectrum is not altered much when L^C is dissolved in water at pH = 10.5, where $[L^C\text{-}2H]^{2-}$ is the main species. Upon excitation into the lowest energy $\pi\rightarrow\pi^*$ transition, a strong emission from the $^1\pi\pi^*$ state is observed at 26 828 cm^{-1} for the solution of L^C in methanol (Figure 9), while the emission is less intense in water (25 336 cm^{-1}). Quantum yield determination (Table 8) yielded a value of Q^L = 18.6% in methanol and 5.5% in water (pH = 7), the latter value being practically pH-independent between 6.8 and 12.1 (Figure F6, Supporting Information). The lower quantum yield in water may be related to strong water interaction with the carboxylic groups of L^C, leading to large collisional deactivation upon exchange between bulk water and H-bound water molecules. It is noteworthy that no triplet-state emission is evidenced at room temperature. In the solid state, the fluorescence band originating from the singlet state is shifted 4000 cm^{-1} toward lower energy (22 745 cm^{-1} at 77 K) compared to the solution in methanol, while a distinct, well-structured emission band from the $^3\pi\pi^*$ state is seen at 10 K (Figure F7, Supporting Information). The 0-phonon transition is located at 20 580 cm^{-1}, and the vibrational progression amounts to 1330 ± 80 cm^{-1}, corresponding to a ring breathing mode (1450 cm^{-1} in the fundamental state). The close proximity of the $^3\pi\pi^*$ and $^1\pi\pi^*$ states (ca. 2200 cm^{-1} in the solid state) is usually not favorable for a good yield of the intersystem crossing,[70] but on the other hand, the $^3\pi\pi^*$ lifetime was determined to be 776 ± 10 ms, a value considerably longer than the lifetimes measured for L^A and L^B (4.4[29] and 4.2[30] ms, respectively) and favorable for an efficient ligand-to-metal energy transfer.

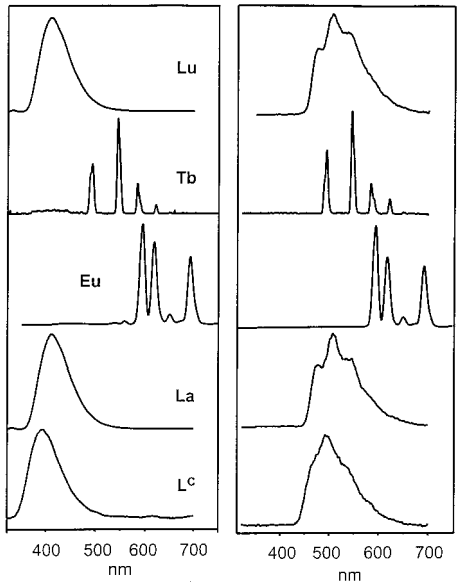

Figure 9. Emission spectra. (Left) Aqueous solutions of 1.1×10^{-5} M $(L^C)^{2-}$ (pH =10.5, $\tilde{\nu}_{exc}$ = 32 570 cm^{-1}) and 4×10^{-6} M $[Ln_2(L^C\text{-}2H)_3]$ (5×10^{-7} M for Tb, pH ≈ 7, $\tilde{\nu}_{exc}$ = 30 120 cm^{-1}) at 295 K. (Right) Frozen solutions in MeOH (10^{-5}−10^{-6} M, 77 K), $\tilde{\nu}_{exc}$ = 32 260 (ligand) and 30 300 cm^{-1} (complexes), phosphorescence mode with time delay of 8 (L^C), 20 (La), 1 (Eu) 0.02 (Tb), and 10 (Lu) ms. Vertical scale: arbitrary units.

(69) Forsberg, J. H.; Delaney, R. M.; Zhao, Q.; Harakas, G.; Chandran, R. *Inorg. Chem.* **1995**, *34*, 3705.

Table 8. Absolute Quantum Yield of the Ligand-Centered Fluorescence in $[Ln_2(L^C\text{-}2H)_3]\cdot nH_2O$ Measured with Respect to 3×10^{-5} M Quinine Sulfate in 0.05 M H_2SO_4

compd	solvent	c/M	$\tilde{\nu}_{exc}$/cm^{-1}	$\epsilon(\tilde{\nu}_{exc})$/ M$^{-1}\cdot$cm^{-1}	Q^L [a]
L^C	MeOH	7.7×10^{-7}	31 546	56 104	0.186
La (**7**)	MeOH	3.9×10^{-6}	30 488	90 541	0.393
Gd (**13**)	MeOH	3.9×10^{-6}	30 211	94 649	0.022
Eu (**14**)	MeOH	2.2×10^{-6}	30 303	98 045	0.0015
Tb (**15**)	MeOH	2.5×10^{-6}	30 211	97 408	0.0015
Lu (**19**)	MeOH	3.9×10^{-6}	30 120	90 141	0.382
L^C	H_2O, pH = 7[b]	8.5×10^{-7}	31 546	44 590	0.055
La (**7**)	H_2O, pH = 6.8	5.0×10^{-7}	30 303	91 400	0.30
Gd (**13**)	H_2O, pH = 6.8	3.9×10^{-6}	30 211	91 865	0.0093
Eu (**14**)	H_2O, pH = 6.8	5.1×10^{-7}	30 303	86 078	[c]
Tb (**15**)	H_2O, pH = 6.8	5.5×10^{-7}	30 120	98 142	0.0005
Lu (**19**)	H_2O, pH = 6.8	4.2×10^{-6}	30 120	97 962	0.289

[a] Average of at least two determinations using different excitation energy for quinine sulfate: 31 645 cm^{-1} (ϵ = 8960 M$^{-1}\cdot$cm^{-1}) and 28 985 cm^{-1} (ϵ = 10 598 M$^{-1}\cdot$cm^{-1}). Estimated error, ±10%. [b] The quantum yield is independent of pH between 6.8 and 12.1. [c] Too weak to be measured.

Upon complexation, the $\pi\rightarrow\pi^*$(C=O) band shifts 1500 cm^{-1} to higher energy with respect to $[L^C\text{-}2H]^{2-}$, while the lower energy $\pi\rightarrow\pi^*$ transition undergoes a red shift of approximately the same magnitude with, in addition, the appearance of a second shoulder on its high-energy side (Figure F5, Supporting Information). The emission from the $^1\pi\pi^*$ state of the ligand is only slightly shifted to lower energy and is visible for all the nonluminescent lanthanide ions and, very faintly, for Eu^{III} and Tb^{III} (Figure 9). This is not the case for the luminescence of the $^3\pi\pi^*$ state, which disappears completely for these two helicates, indicating sensitization of the metal ions via a $^3\pi\pi^*$-to-metal energy transfer. The 0-phonon transition of the $^3\pi\pi^*$ emission somewhat shifts to lower energy, from 21 050 (La) to 20 660 cm^{-1} (Gd, Lu), as a consequence of the greater charge density exhibited by the heavier ions over La^{III} and resulting in stronger Ln−X bonds, while the lifetime is considerably reduced, to 246 ± 2, 181 ± 6, and 7.3 ± 0.1 ms for La, Lu, and Gd, respectively. The ligand-centered fluorescence is somewhat enhanced in solutions of the La^{III} and Lu^{III} helicates in methanol compared with that of the free ligand. This enhancement may be understood because complexation rigidifies the ligand, which loses internal degrees of freedom with, as a consequence, less efficient vibrational deactivation processes. In water, the effect of complexation is more dramatic, and Q^L increases more than 5-fold to reach 55% and 53% for the La^{III} and Lu^{III} helicates. The Gd^{III} helicate behaves quite differently, with a large decrease in the ligand-centered fluorescence both in methanol and water. Since other data do not reveal a structural change for the Gd^{III} helicate between solid state and solution, the observed quenching of the ligand-centered emission and the shortening of the $^3\pi\pi^*$ lifetime must arise from interaction with the paramagnetic ($S = {}^7/_2$) electronic structure of the Gd^{III} ion, as has been pointed out for other complexes.[6] Finally, it is noteworthy that some $^1\pi\pi^*$ fluorescence is observed for both the Eu^{III} and Tb^{III} helicates, pointing to an incomplete $^1\pi\pi^*\rightarrow{}^3\pi\pi^*\rightarrow{}^5D_J$ energy transfer; the remaining fluorescence is, however, quite weak, about 0.2% of the $^1\pi\pi^*$ emission of the Eu^{III} and Tb^{III} helicates in methanol. In water, this share is even smaller, about 0.1% for Tb^{III}, while it almost completely vanishes for Eu^{III}.

Metal-Centered Luminescence of $[Eu_2(L^C\text{-}2H)_3]$ (13) and $[(Ln_{1.96}Eu_{0.04})(L^C\text{-}2H)_3]$ (Ln = La, 20; Lu, 21) in the Solid State. Since the Eu helicate is strongly luminescent, we have examined its properties in the solid state at 295, 77, and 10 K for the purpose of investigating the coordination environment around the luminescent ion and analyzing the energy migration pathways. The excitation spectrum of $[Eu_2(L^C\text{-}2H)_3]$ (**13**) at 10 K produces a broad and intense band with a maximum at 27 250 cm^{-1}, corresponding to excitation to the lowest $^1\pi\pi^*$ ligand state, in addition to weak and sharp bands reflecting direct metal excitation to the ^5D_J levels (J = 0, 1, and 2). The emission spectrum obtained upon excitation through ligand level (Figure 9; Figure F8 and Table S20, Supporting Information) is characteristic of Eu^{III} rigid environments close to D_3 symmetry.[29] The $^5D_0\rightarrow{}^7F_0$ transition appears at 17 221 cm^{-1} with a shoulder at 17 230 cm^{-1}, a finding confirmed by the high-resolution laser-excited excitation spectrum of the $^5D_0\leftarrow{}^7F_0$ transition, which reveals two sharp components at 17 223 cm^{-1} (site I, full width at half-height, fwhh = 3.3 cm^{-1}) and 17 229 cm^{-1} (site II, fwhh = 5.1 cm^{-1}) (Figure F9, Supporting Information). Selective laser excitation on these two components yields very similar spectra (Figures F8 and F10, Supporting Information), preventing a population analysis based on the $^5D_0\rightarrow{}^7F_1$ transition.[71] The Eu($^5D_0$) lifetimes of sites I and II are long, 2.69 ± 0.01 and 2.47± 0.01 ms, respectively, and preclude the presence of a water molecule in the inner coordination sphere. They are almost temperature-independent between 10 and 295 K, pointing to rigid environments for Eu^{III}. Both the variation in lifetime and the slight crystal field splitting changes observed between sites I and II point to second-sphere effects that we assign to interaction of water molecules with the ligand strands via H-bonding, thus distorting the general coordination sphere of the Eu^{III} ion, as observed in $[Eu_2(L^A)_3]^{6+}$.[29] From the spectra of $[Eu_2(L^C\text{-}2H)_3]$ at 10 K, the two components of the transition to the $^7F_1$(E) level are calculated to be 70 (site I) and 56 (site II) cm^{-1} apart (Table 11). The spacing of the E doublet reflects the amount of distortion with respect to the idealized symmetry,[72] and the distortion in the helicates with L^C appears to be more important than that for the corresponding edifices with L^A [29] and L^B.[30] On the other hand, the metal ion is better protected against nonradiative de-excitation, the lifetime being longer, ca. 2.5 versus ca. 2 ms. The overall shape of the emission spectra of $[(Ln_{1.96}Eu_{0.04})(L^C\text{-}2H)_3]$ (Ln = La, **20**; Lu, **21**) remains similar with respect to the that of pure homodinuclear helicate **13** (Figure F11, Supporting Information). Detailed examination of the crystal field splittings displays, however, some differences. For Ln = La, the two different sites yield spectra similar to those of the Eu helicate, while the emission spectrum of the Lu edifice reflects a local symmetry closer to the idealized D_3 symmetry. This finding is compatible with the differences in the solution structures unraveled by NMR spectroscopy. The lifetimes of the $^5D_0$ excited state, measured under broad-band excitation through the ligand levels, are identical at 10 K for both the La^{III} and Lu^{III} helicates, 3.03 ± 0.07 ms, and they are longer compared to the lifetime recorded for the pure homodimetallic Eu^{III} helicate (2.67 ± 0.04 ms). Their temperature dependence is nevertheless different, leading to a value of 2.72 ± 0.01 ms for La at 295 K compared to 2.13 ± 0.02 ms for Lu and 2.43 ± 0.01 ms for the homodimetallic edifice. These differences reflect varying contributions of the nonradiative deexcitation processes and shorter Ln−X distances favoring larger coupling with vibrational functions.

Metal-Centered Luminescence in $[Tb_2(L^C\text{-}2H)_3]$ (15) and $[(EuTb)(L^C\text{-}2H)_3]$ (22). The weak emission spectrum arising from the Tb^{III} centers of helicate **15** is dominated by the $^5D_4\rightarrow{}^7F_5$

(70) Steemers, F. J.; Verboom, W.; Reinhoudt, D. N.; Vandertol, E. B.; Verhoeven, J. W. *J. Am. Chem. Soc.* **1995**, *117*, 9408.
(71) Verwey, J. W. M.; Blasse, G. *Chem. Mater.* **1990**, *2*, 458.

transition, and the lifetime of the $^5D_4$(Tb) state follows a somewhat unusual pattern, increasing from 1.91 ± 0.03 ms at 10 K to 2.10 ± 0.02 ms at 100 K and then sharply decreasing to 50 μs at 270 K (room-temperature luminescence is too faint for allowing the determination of τ). This is characteristic of a complex in which a $Tb^{III} \rightarrow L^C$ energy back-transfer occurs as a result of the low energy of the ligand $^3\pi\pi^*$ state (cf. the component at 16 560 cm^{-1} in the ligand-centered phosphorescence spectrum of $[Gd_2(L^C\text{-}2H)_3]$) compared to the energy of the $^5D_4$(Tb) state (18 380 cm^{-1}). The lifetime decay for $[Tb_2(L^C\text{-}2H)_3]$) is exponential with respect to the temperature, and an Arrhenius type analysis[73] (Figure F12, Supporting Information) yields an activation energy of 1226 ± 25 cm^{-1}, indicating a back-transfer assisted by ligand vibrations. The $[(EuTb)(L^C\text{-}2H)_3]$ compound, which consists of a mixture of the two homodimetallic helicates and of the heterodimetallic edifice, displays both Eu^{III} and Tb^{III} luminescence below 150 K and Eu^{III} luminescence only above this temperature. The Eu($^5D_0$) lifetime is identical with that measured for the homodimetallic helicate **13**, while the Tb($^5D_4$) lifetime is shorter than that in $[Tb_2(L^C\text{-}2H)_3]$, 1.78 ± 0.09 vs 2.12 ± 0.02 ms at 77 K, reflecting a Tb^{III}-to-Eu^{III} energy transfer. Due to the weak luminescence of the Tb^{III} ion, we could not separate the lifetime of the luminescence arising from the homodimetallic helicate from that of the heterodimetallic edifice, except at 120 K, where the luminescence decay can be analyzed in terms of a biexponential function with lifetimes equal to 1.39 ± 0.01 (homodimetallic edifice) and 0.25 ± 0.01 ms (heterodimetallic helicate). At this temperature, the yield of the Tb-to-Eu energy transfer, which is equal to $(1 - \tau/\tau_0)$, where τ_0 is the lifetime without acceptor, amounts to 82%. Assuming that the energy-transfer mechanism is of dipole−dipole nature,[1] an estimation of r_0, the distance for which the energy transfer yield amounts to 50%, yields r_0 = 11.5 Å, a value comparable to that calculated for $[EuTb(L^A)_3]^{6+}$ (10.4 Å).[29]

$$\eta = 1 - \tau/\tau_0 = [1 + (r_{DA}/r_0)^6]^{-1} \qquad (9)$$

Metal-Centered Luminescence of $[Eu_2(L^C\text{-}2H)_3]$ in Solution. Upon ligand excitation, solutions of 3×10^{-4} M **13** in H_2O and D_2O display identical intense emission spectra, the overall shapes of which are similar to the emission spectrum of the solid sample (Figure F8, Supporting Information). The $^5D_0 \rightarrow {}^7F_0$ transition occurs as a single symmetrical and broad band at 17 232 cm^{-1} (fwhh = 15 cm^{-1}). The emission bands are relatively broad, which offsets crystal field splittings, and therefore the emitting species appears to be more symmetrical than in the solid state. In particular, the $^5D_0 \rightarrow {}^7F_1$ and $^5D_0 \rightarrow {}^7F_2$ transitions display only two components, while four components are observed for $^5D_0 \rightarrow {}^7F_4$, in perfect agreement with the D_3 symmetry reflected in the NMR spectra. The $^5D_0$ lifetime is as long as that in the solid state, 2.43 ± 0.02 ms in H_2O, a value which increases slightly to 2.53 ± 0.02 ms upon dilution to 3×10^{-8} M. It is noteworthy that no dissociation occurs at this concentration, as exemplified by the relative intensities of the $^5D_0 \rightarrow {}^7F_J$ transitions, which remain constant compared to those of the 3×10^{-4} M solution. For a 10^{-6} M solution in D_2O, the lifetime amounts to 4.66 ± 0.02 ms and does not vary upon dilution to 10^{-10} M. Using Horrock's equation for the calculation of the number q of coordinated water molecules,[1]

$$q = 1.05(k_{H_2O} - k_{D_2O}) \qquad (\text{with } k \text{ in } ms^{-1}) \qquad (10)$$

we find $0.19 < q < 0.21$. If we use the correction proposed by Parker, who takes into account the second-sphere contribution of closely diffusing OH oscillators by subtracting somewhat empirically 0.25 ms^{-1} to Δk, q vanishes, which proves that the Eu^{III} ions are completely protected from direct water interaction, even at high dilution, and points to a good Eu^{III}-containing luminescent probe. The quantum yield of the metal-centered luminescence upon ligand excitation amounts to 1.34% (pH = 6.9) for Eu and 0.20% for Tb (pH = 7.3; Table S21, Supporting Information). A plot of the intensity of the $^5D_0 \rightarrow {}^7F_2$ transition versus the concentration of the Eu helicate shows a detection limit around 10^{-9} M in H_2O (Figure F13, Supporting Information) and 10^{-11} M in D_2O.

Discussion

Self-Assembly Process and Solid-State Structure. The ditopic dicarboxylic ligand L^C has been coded for the coordination of two nine-coordinate lanthanide ions in tricapped trigonal prismatic environments. The methylene bridge allows the two tridentate compartments of the ligand to adopt a twisted conformation, leading to the formation of triple-stranded dimetallic helicates in which the trivalent lanthanide ions are tightly bound. Spectroscopic data show that strict self-assembly takes place in water, leading to the formation of 18 ion−ion and ion−dipole bonds with concomitant desolvation of the Ln^{III} ions. One remarkable feature is that the large hydration energy of the trivalent lanthanide ions is more than overcome by the thermodynamic contribution of the self-assembly process, resulting in very stable edifices.

From the available crystal data on the Eu and Tb helicates, we see that the wrapping of the three ligand strands in $[Ln_2(L^C\text{-}2H)_3]$ is mainly governed by ion−dipole interactions, since aromatic $\pi-\pi$ interactions seemingly play no role in these edifices, as already noted for both the homodimetallic edifices with L^A [29] and L^B [30] and the heterodimetallic triple-stranded helicate $[EuZn(L^{II})_3]^{5+}$.[21] The rigid benzimidazole and pyridine moieties of the ditopic ligands L^A, L^B, and L^C prevent them from folding too tightly, resulting in dimetallic triple-stranded helicates with relatively long and similar pitches (24−25 Å). The carboxylate end groups of ligand L^C are firmly bound to the metal ion, precluding any direct interaction with water molecules, both in the solid state and in solution. The introduction of two different types of donor atoms in the coordination polyhedra of the metal ions in the helicates with L^B and L^C introduces more distortion from the idealized D_{3h} symmetry, compared with $[Eu_2(L^A)_3]^{6+}$,[29] the distortion increasing further on going from the helicates with L^B to the edifices with L^C. Part of the distortion is traceable to the large number of second-sphere interactions occurring in $[Ln_2(L^C\text{-}2H)_3]$ through H-bonds with water molecules. However, the chemical environment around the Eu^{III} ions in $[Ln_2(L^C\text{-}2H)_3]$ remains sufficiently close to a trigonal symmetry to be reflected in the crystal-field splitting, as evidenced in the metal-centered luminescence spectra. As far as the solid-state structure is concerned, the general arrangement is maintained along the lanthanide series, but emission spectra of Eu-doped helicates point to some differences between La and Eu on one side and Lu on the other side. The decrease in the ionic radius on going from La^{III} to Lu^{III} induces a stronger Ln−X interaction, which attracts the carboxylate group closer to the metal ion and which, as a consequence, causes the ligand strands to unwrap somewhat.

(72) Bünzli, J.-C. G.; Piguet, C. In *Syntheses and Methodologies in Inorganic Chemistry*; Daolio, S., Tondello, E., Vigato, P. A., Eds.; Università degli Studi di Padova: Padova, Italy, 1996.

The X-ray structure of the $[Yb_2(L^C\text{-}2H)_3]$ helicate substantiates this reasoning. The monoclinic crystals were not of sufficient quality, but reliable data could be obtained for the Yb···Yb distance and for the Yb^{III} coordination polyhedra. The crystallographic space group is $P2_1/c$, and the overall structure is very similar to those determined for Eu^{III} and Tb^{III}, with two distinct types of molecules and extensive second-sphere interactions with water molecules. With respect to the Eu^{III} helicate, the metal−metal distance increases by 0.26−0.30 Å (molecules A, 9.11 Å; molecules B, 9.32 Å); the Ln−N(py) and Ln−N(bz) mean distances are the same, 2.57 and 2.64 Å, respectively, but the mean Ln−O distance sustains a sizable reduction from 2.40 (Eu) to 2.35 Å (Yb).

Solution- versus Solid-State Structure of the $[Ln_2(L^C\text{-}2H)_3]$ Helicates. According to Kemple et al.,[66] substitution of Bleaney's coefficients C_j[74] by a direct determination of the magnetic susceptibility tensor will improve considerably the separation of contact and dipolar contributions to the LIS. To calculate the latter, we have determined the axial coordinates r_i^n and θ_i^n ($n = 1, 2$; Scheme 3) of the protons $H^{4'}$, $H^{6'}$, $H^{7'}$, H^3, H,[4] H^5, and b-CH_2 from the X-ray structure of the Eu^{III} helicate, using the Eu−Eu 3-fold axis as the magnetic z axis.[66] D_3 symmetry is obtained by averaging the axial coordinates of symmetry-related protons. The experimental isotropic lanthanide-induced shifts for these protons have been fitted to eq 11, which takes into account the contribution of both metallic centers to the pseudocontact shifts with five parameters for each Ln^{III} ion: the experimental axial anisotropic susceptibility parameter $\xi\chi_j^{zz}$ and four δ_{ij}^c contributions for $H^{4'}$, H^{3-5} (7×5 fit).[66]

$$\delta_{ij}^{para} = \xi\chi_j^{zz}\left(\frac{1 - 3\cos^2\theta_i^1}{(r_i^1)^3} + \frac{1 - 3\cos^2\theta_i^2}{(r_i^2)^3}\right) + \sum_{i=H^{4'},H^3,H^4,H^5} \delta_{ij}^c \qquad (11)$$

This mathematical treatment results in agreement factors quite lower than the factors calculated with Reilley's method (Table 7; Tables S23 and S24, Supporting Information). For the series Ce−Tb, the F_i and G_i^{global} values calculated from δ_{ij}^c and δ_{ij}^{pc} and eqs 4 and 5 are in qualitative good agreement with those extracted previously, except for $H^{4'}$, which is close to the paramagnetic center and whose G_i^{global} terms are extremely sensitive to small structural variations. We conclude that $[Eu_2(L^C\text{-}2H)_3]\cdot 20.5H_2O$ is a good structural model for these helicates in solution. For the Er−Yb series, the G_i^{global} values are also similar to those determined using Reilley's method, pointing to only minor structural changes between the two isostructural series. This statement is confirmed by the good match observed between the theoretical C_j values of the Bleaney's coefficient and the experimental axial component of the anisotropic susceptibility ($\xi\chi_j^{zz}$) obtained for the helicates $[Ln_2(L^C\text{-}2H)_3]$ along the complete lanthanide series (Table S22, Supporting Information). The effects of the paramagnetic center on the NMR longitudinal (T_1) relaxation processes are accounted for by the Solomon−Bloembergen−Morgan equation,[75,76] which is reduced to dipolar and Curie spin contributions for lanthanide complexes because contact contributions are negligible:

$$\frac{1}{T_1^i} = \frac{4}{3}\frac{\gamma_I^2\mu_{eff}^2}{r_i^6}T_{1e} + \frac{1}{5}\frac{\gamma_I^2\mu_{eff}^4 H_0^2}{(3kT)^2 r_i^6}\left(\frac{6\tau_r}{1+\omega^2\tau_r^2}\right) \qquad (12)$$

As both remaining contributions depend on r_i^{-6}, the use of a nucleus sufficiently remote from the paramagnetic center as an internal reference[77] reduces eq 12 to its simplest form, corrected for diamagnetism,[60] in which k_i^{tot} and k_i^{dia} are the longitudinal relaxation rates measured for the nucleus i in the paramagnetic complex and its diamagnetic analogue, respectively, and r_i is the Ln−nucleus i distance:

$$\frac{k_{ref}^{tot} - k_{ref}^{dia}}{k_i^{tot} - k_i^{dia}} = \left(\frac{r_i}{r_{ref}}\right)^6 \qquad (13)$$

For the dimetallic complex $[Ln_2(L^C\text{-}2H)_3]$, each nucleus undergoes the sum of two dipolar paramagnetic contributions to their longitudinal relaxation rate. So that the total relaxation rate k_i^{tot} is given by eq 14, in which r_i^n are the Ln^n−nucleus i distance, P is a constant depending on the magnetic properties of the paramagnetic complex and on external conditions (T, H_0) and k_i^{dia} is the diamagnetic contribution obtained for $[La_2(L^C\text{-}2H)_3]$:

$$k_i^{tot} - k_i^{dia} = (k_i^{para})_{site1} + (k_i^{para})_{site2} = P\left(\frac{(r_i^1)^6 + (r_i^2)^6}{(r_i^1)^6(r_i^2)^6}\right) \qquad (14)$$

The consideration of an internal reference leads to eq 15, which replaces eq 13 for dimetallic lanthanide complexes.

$$\frac{k_{ref}^{tot} - k_{ref}^{dia}}{k_i^{tot} - k_i^{dia}} = \left(\frac{(r_{ref}^1)^6 + (r_{ref}^2)^6}{(r_i^1)^6 + (r_i^2)^6}\right)\left(\frac{(r_i^1)^6(r_i^2)^6}{(r_{ref}^1)^6(r_{ref}^2)^6}\right) \qquad (15)$$

Taking the r_i^n distances observed in the crystal structure of $[Eu_2(L^C\text{-}2H)_3]\cdot 20.5H_2O$ (Table 7) and H^5 as an internal reference, we have calculated the expected ratios $(k_{ref}^{tot} - k_{ref}^{dia})/(k_i^{tot} - k_i^{dia})$. The differences between the two approaches (eqs 13 and 15) are minor for protons H^3, H^4, H^5, and $H^{4'}$ (<2.5%) because r_i^1 and r_i^2 are sufficiently different and the contribution of one paramagnetic metal ion dominates. Equation 13 can be thus used to extract the approximate Ln−H^i distances ($i = 3-5$) collected in Table 9 (see also Table S25, Supporting Information). For $H^{6'}$, $H^{7'}$, and b-CH_2, r_i^1 and r_i^2 are comparable, eq 15 holds, and no straightforward estimation of the Ln−H^i distances is available. On the other hand, the comparison of the experimental $[(k_{ref}^{tot} - k_{ref}^{dia})/(k_i^{tot} - k_i^{dia})]_{exp}$ ratios obtained from the relaxation measurements with that calculated from the X-ray crystal structure of the Eu^{III} helicate shows a satisfying concordance for Ce^{III}, Pr^{III}, and Nd^{III}, hence confirming that $[Eu_2(L^C\text{-}2H)_3]\cdot 20.5H_2O$ is a good structural model. However, the significant deviations obtained for $H^{6'}$ and $H^{7'}$ in the Yb^{III} helicate point to a somewhat different structure for this edifice, in complete agreement with the observation of two isostructural series in solution for large and small Ln^{III} and with the partial solid-state structural data obtained for the Yb^{III} helicate, showing a slight lengthening of the metal−metal distance compared to those in the Eu^{III} and Tb^{III} helicates.

Photophysical Properties. The experimental energy of the $^5D_0 \leftarrow {}^7F_0$ transition may be rationalized using the phenomenological relationship proposed by Frey and Horrocks,[78] who

(73) Kleinerman, M.; Choi, S.-I. *J. Chem. Phys.* **1968**, *49*, 3901.
(74) Bleaney, B. *J. Magn. Reson.* **1972**, *8*, 91.
(75) Luchinat, C. *Acc. Chem. Res.* **1998**, *31*, 351.
(76) Aime, S.; Botta, M.; Parker, D.; Williams, J. A. G. *J. Chem. Soc., Dalton Trans.* **1995**, 2259.
(77) Brink, J. M.; Rose, R. A.; Holz, R. C. *Inorg. Chem.* **1996**, *35*, 2878.
(78) Frey, S. T.; Horrocks, W. deW., Jr. *Inorg. Chim. Acta* **1995**, *229*, 383.

Table 9. Ln−H Distances in 10^{-2} M $[Ln_2(L^C\text{-}2H)_3]$ Solutions in D_2O (7.4 < pD < 8.5) Calculated from Corrected Experimental Relaxation Times (T_1) Using Eq 13 and Normalized to the Eu−H^5 Distance[a]

Ln		$H^{6'}$	$H^{7'}$	b-CH_2	H^3	H^4	H^5
Ce	T_1/ms	1235	1212	886.7	361.0	928.7	415.6
	r_i^1/Å				5.30	6.20	5.42
Pr	T_1/ms	620.7	589.6	390.3	163.5	395.8	193.1
	r_i^1/Å				5.27	6.11	5.42
Nd	T_1/ms	550.4	481.5	373.3	182.2	290.5	165.9
	r_i^1/Å				5.51	6.07	5.42
Yb	T_1/ms	369.9	342.6	187.3	93.2	198.0	87.1
	r_i^1/Å				5.48	6.21	5.42
Eu (RX)	r_i^1/Å	7.27	6.82	6.53	5.55	6.27	5.42
Ce	$[(k_{ref}^{tot} - k_{ref}^{dia})/(k_i^{tot} - k_i^{dia})]_{exp}^b$	2.98	2.93	2.02	0.87	2.23	1
Pr	$[(k_{ref}^{tot} - k_{ref}^{dia})/(k_i^{tot} - k_i^{dia})]_{exp}^b$	3.05	3.21	2.13	0.85	2.05	1
Nd	$[(k_{ref}^{tot} - k_{ref}^{dia})/(k_i^{tot} - k_i^{dia})]_{exp}^b$	3.33	2.90	2.25	1.10	1.97	1
Yb	$[(k_{ref}^{tot} - k_{ref}^{dia})/(k_i^{tot} - k_i^{dia})]_{exp}^b$	4.24	3.93	2.15	1.07	2.77	1
Eu (RX)	$[(k_{ref}^{tot} - k_{ref}^{dia})/(k_i^{tot} - k_i^{dia})]_{calc}^b$	2.95	2.91	2.10	1.12	2.35	1

[a] $H^{4'}$ has been excluded because of its large relaxation rate. [b] According to eqn 15 with H^5 as an internal reference, see text.

showed that a correlation exists between the energy of the 0−0 transition, that is, the position of the $^5D_0$ level, and parameters describing the ability δ of coordinating atoms to produce a nephelauxetic effect:

$$\tilde{\nu} - \tilde{\nu}_0 = C_{CN}\sum_i n_i\delta_i \qquad (16)$$

where C_{CN} is a coefficient depending upon the Eu^{III} coordination number (1.0 for CN = 9), n_i the number of atoms of type i, and $\tilde{\nu}_0$ = 17 374 cm^{-1} at 295 K. Using $\delta_{OOCR} = -17.2$ (ref 78) and the nephelauxetic parameter deduced from our previous studies on heterocyclic imines, $\delta_{N=C} = -15.3$, we predict $\tilde{\nu}$ = 17 231 cm^{-1}, in very good agreement with the measured value of 17 229 cm^{-1} for the main component of the 0−0 transition at 295 K. We also note that the values found for $[(Ln_{1.96}Eu_{0.04})\text{-}(L^C\text{-}2H)_3]$ (Ln = La, Lu) closely match the calculated energy.

According to the low-temperature (185 K) molecular X-ray structure determined for **13a**, there are two types of molecules, A and B, and four different metal ion sites. At low temperatures, we find two slightly different metal ion environments (sites I and II), so that two (or more) of the four Eu^{III} sites apparently display almost identical photophysical properties. Assignment of these sites can be made by considering the detailed chemical environment of the four Eu^{III} ions. The mean Eu−X (X = O, N) distances differ only marginally for the four metal ion sites (Table 4), which explains the very similar total ligand field splitting of $^7F_1$ for both sites I and II. Analysis of the coordination polyhedra and of the general arrangement of the ligand strands shows molecules B being more distorted than molecules A, with a different arrangement of the ligand strands, and from this point of view, assignment of site I, which displays a larger distortion from the idealized D_3 symmetry compared to site II, to molecules B seems reasonable. The lengthening of the $^5D_0$ lifetime of Eu^{III} ions in site I by ca. 8% over the lifetime recorded for ions in site II can be explained by inspecting the extensive network of second-sphere interactions with water molecules (Figure 7; Table S16, Supporting Information): on average, the O···O contacts are slightly shorter in molecules A, which induces a more effective nonradiative de-excitation. Second-sphere hydrogen-bonded water molecules have, indeed, been shown to contribute to the rate constant $1/\tau$ for depopulation of the $^5D_0$ excited state.[79]

Several criteria have been tested recently for predicting the effectiveness of the antenna effect in Eu^{III}- and Tb^{III}-containing edifices. From their work on sensitizer-modified calix[4]arenes, Reinhoudt and co-workers concluded that the 0-phonon band of the ligand triplet state must be 3500 cm^{-1} above the Ln excited state to ensure efficient energy transfer. The same authors also point to the fact that the $^1\pi\pi^* \rightarrow {}^3\pi\pi^*$ intersystem crossing is maximized when the energy difference between these states amount to ca. 5000 cm^{-1}.[70] In another investigation, Latva et al.[80] have determined the luminescence quantum yields of 41 Eu and Tb chelates as a function of the energy of the $^3\pi\pi^*$ 0-phonon transition of the ligand and reached a similar conclusion, the best efficiency in energy transfer being obtained when the 0-phonon transition lies around 21 000−22 000 cm^{-1}. On the other hand, efficient back-transfer takes place in Tb^{III}-containing compounds when $\Delta E(^3\pi\pi^* - {}^5D_4) < 1850$ cm^{-1}. Finally, we have recently shown that the LMCT state plays a crucial role in deactivating the Eu-centered luminescence in the triple-helical complex $[Eu(L^1)_3]^{3+}$.[10] Comparing the Eu^{III} and Tb^{III} sensitization in the three series of dimetallic helicates with L^A, L^B, and L^C using these criteria leads to the following considerations. The 0-phonon transition of the ligand $^3\pi\pi^*$ state (as measured at 77 K on the Gd complexes) lies at 19 880 (L^A), 20 930 (L^B), and 20 660 (L^C) cm^{-1}, resulting in $^1\pi\pi^* - {}^3\pi\pi^*$ energy differences of respectively 6090, 4510, and 4570 cm^{-1}, that is, for the last two data, somewhat small for an efficient intersystem crossing. This is probably the reason a faint $^1\pi\pi^*$ emission is still visible in the $[Ln_2(L^C\text{-}2H)_3]$ (Ln = Eu, Tb) helicates. The $\Delta E(^3\pi\pi^* - {}^5D_0)$ energy differences amount to 2650 (L^A), 3700 (L^B), and 3430 (L^C) cm^{-1}, while the $\Delta E(^3\pi\pi^* - {}^5D_4)$ gap is either negative (L^A) or smaller than 500 cm^{-1} (L^B, L^C). This easily explains the absence (L^A) or the very poor sensitization of Tb^{III} in the three helicates. The quantum yields of the Eu-centered luminescence amounts to 6.5×10^{-5} (L^A, MeCN), 3.5×10^{-3} (L^B, MeCN), and 1.3×10^{-2} (L^C, H_2O). The first figure cannot be simply rationalized from the data calculated above, and, in view of the similarity of the Eu^{III} environments in $[Eu_2(L^A)_3]^{6+}$ and $[Eu(L^1)_3]^{3+}$, it is reasonable to invoke a low-lying LMCT state to explain the extremely poor luminescence efficiency of the dimetallic helicate with L^A.[10] This is substantiated by the fact that the $^5D_0$ lifetime in $[Eu_2(L^A)_3]^{6+}$ is temperature-dependent, while it is not in the edifices with L^B and L^C, suggesting a blue shift of the LMCT state in the latter two compounds. The 4-fold increase in the quantum yield of $[Eu_2(L^C\text{-}2H)_3]$ (in water) over $[Eu_2(L^B)_3]^{6+}$ (in acetonitrile) cannot be explained by the above-mentioned criteria, since both the $^1\pi\pi^* - {}^3\pi\pi^*$ and $^3\pi\pi^* - {}^5D_0$ energy differences are comparable for both edifices. This points to the difficulty in predicting antenna effects in Ln-containing materials, mainly due to the fact that interacting electronic levels have very different widths, the ligand $^1\pi\pi^*$ and $^3\pi\pi^*$ states extending over several thousands of cm^{-1}, while Ln^{III} levels span only a few tens of cm^{-1}. Therefore, a very slight shift in the ligand $^3\pi\pi^*$ level and/or a slight difference in the respective intensity of its vibronic components can substantially affect the overlap integral

(79) Beeby, A.; Clarkson, I. M.; Dickins, R. S.; Faulkner, S.; Parker, D.; Royle, L.; de Sousa, A. S.; Williams, J. A. G.; Woods, M. *J. Chem. Soc., Perkin Trans. 2* **1999**, 493.

(80) Latva, M.; Takalo, H.; Mukkala, V. M.; Matachescu, C.; Rodriguez-Ubis, J.-C.; Kankare, J. *J. Luminesc.* **1997**, *75*, 149.

with the lanthanide 4f functions and, consequently, the yield of the energy transfer.

Conclusions and Perspectives

Ligands bearing polyaminocarboxylate groups are widely used in coordination chemistry and particularly in lanthanide chemistry because they form unusually stable and water-soluble complexes. Landmarks in this field are the multidentate ligand edta, on which highly accurate complexometric titration methods are based,[81] and the macrocyclic ligand dota, used to encapsulate the Gd^{III} cation in contrast agents for MRI.[2] Bifunctional chelating agents have been recently developed for antibody or antigen labeling which are based on modified edta molecules.[4] On the other hand, due to its chemical nature, dota is not easy to modify if the carboxylic acid functions are to be retained. In this paper, we propose a third class of polyaminocarboxylic ligands, of which the first member L^C presents the following advantages and properties: (i) the ligand is ditopic, featuring two tridentate moieties, and is therefore coded for the coordination of two Ln^{III} cations; (ii) the receptor has been designed to form structurally defined dimetallic triple-stranded helicates by self-assembly; (iii) the stability of the resulting edifices is large enough to offset the considerable hydration enthalpy of the Ln^{III} ions, so that formation of the complexes can take place in water; (iv) the helicates are stable between pH = 4 and 13; (v) the metal ions are well protected from external interaction, even from small molecules such as water; and (vi) the ligand is amenable to easy functionalization, which will allow a fine-tuning of the physicochemical properties of the helicates.

Thermodynamic strict self-assembly of L^C with Ln^{III} ions produces triple-stranded dimetallic helicates with pseudo-D_3 symmetry both in the solid state and in solution, the distortion of the Ln^{III} coordination polyhedra being smaller in the latter. The wrapping of the ligand strands around the metal ions offers sufficient flexibility to produce very stable edifices with all the lanthanide ions, the reduction in the Ln^{III} size on going from La to Lu being reflected only in a slight elongation of the helix and a tighter coordination of the carboxylate groups. Despite the fact that the initial ligand design used here has focused on producing a simple and robust receptor, ensuring a large thermodynamic stability of the dimetallic edifices, the latter possess interesting photophysical properties: the ligand luminescence can be tuned by the nature of the Ln^{III} ion, and the ligand selectively sensitizes the Eu^{III} luminescence. Although the quantum yield of the europium-centered luminescence remains modest for the L^C helicate in water, there is no doubt that introduction of light-harvesting substituents displaying good antenna effect on the backbone of L^C will considerably enhance the metal-centered luminescence. This is easily conceivable in view of the intrinsic advantages afforded by the flexible synthetic route used to isolate L^C: the asymmetric synthon 6-(*N*,*N*-diethylcarbamoyl)pyridine-2-carboxylic acid (**2**) can be substituted in the 4-position of the pyridine to modulate the electron density on the pyridine N atom, the pK_a of the carboxylic acid, and the light-harvesting properties. This 4-position may also serve to build an activated functional group in the chelating agents, forming covalent linkages with, for instance, the amino groups of a biological molecule.

In conclusion, the dimetallic lanthanide helicates discussed in this paper open the way for the design of an entire class of compounds into which photophysical functionalities can be built, and therefore an interesting potential in labeling and sensing technologies.

Acknowledgment. We gratefully acknowledge Professor John Forsberg for sending us a copy of the SHIFT ANALYSIS program and Ms. Véronique Foiret for her help in obtaining the photophysical data. J.-C.G.B. thanks the Fondation Herbette (Lausanne) for the gift of spectroscopic equipment and Guerbet SA (Paris) for providing a sample of dota. C.P. thanks the Werner Foundation for a fellowship. This work is supported through grants from the Swiss National Science Foundation.

Supporting Information Available: Tables of elemental analyses and IR data for the ligands and complexes; atomic coordinates and equivalent isotropic and anisotropic displacement parameters for $[Tb_2(L^C)_3\text{-}2H)]\cdot 20.5H_2O$ (**15a**); selected distances and angles and a description of the analysis of the coordination polyhedra in both the Eu (**13a**) and Tb (**15a**) helicates; contact distances with water molecules in **13a** and **15a**; computed values for the contact and dipolar shifts of the $[Ln_2(L^C\text{-}2H)_3]$ helicates in water together with relative ratios of the pseudocontact terms; electronic properties of L^C and its helicates; crystal fields splittings, lifetimes, and relative quantum yield of the Eu (**13**) and Tb (**15**) helicates; relaxation times of the $[Ln_2(L^C\text{-}2H)_3$ helicates in water; and figures showing the NMR spectra of L^C in DMSO-d_6 and D_2O; spectrophotometric and ^1H NMR titration of L^C by Eu^{III} in water; plots of δ_{ij}^{para}/C_j vs $\langle S_z\rangle_j/C_j$ and of $\delta_{ij}^{para}/\langle S_z\rangle_j$ vs $C_j/\langle S_z\rangle_j$ for the various protons in $[Ln_2(L^C\text{-}2H)_3]$ in D_2O; absorption spectra of L^C and the helicates in methanol and water; ligand-centered fluorescence and phosphorescence spectra; excitation and emission spectra of the metal-centered luminescence; temperature dependence of the $Tb(^5D_4)$ lifetime; and dependence of the intensity of the Eu-($^5D_0 \rightarrow {}^7F_2$) transition vs concentration (PDF). X-ray crystallographic data for **15a**, in CIF format, are also available. This material is available free of charge via the Internet at http://pubs.acs.org.

JA991854Q

(81) Schwarzenbach, G. *Complexometric Titrations*; Chapman & Hall: London, 1957.